

# Polyelectrolytes in Multivalent Salt Solutions under the Action of DC Electric Fields

Kun-Mao Wu, Yu-Fu Wei, and Pai-Yi Hsiao\*

*Department of Engineering and System Science,*

*National Tsing Hua University, Hsinchu, Taiwan 300, R.O.C.*

(Dated: November 12, 2018)

## Abstract

We study conformational and electrophoretic properties of polyelectrolytes (PEs) in tetravalent salt solutions under the action of electric fields by means of molecular dynamics simulations. Chain conformations are found to have a sensitive dependence on salt concentration  $C_s$ . As  $C_s$  is increased, the chains first shrink to a globular structure and subsequently reexpand above a critical concentration  $C_s^*$ . An external electric field can further alter the chain conformation. If the field strength  $E$  is larger than a critical value  $E^*$ , the chains are elongated.  $E^*$  is shown to be a function of  $C_s$  by using two estimators  $E_I^*$  and  $E_{II}^*$  through the study of the polarization energy and the onset point of chain unfolding, respectively. The electrophoretic mobility of the chains depends strongly on  $C_s$ , and the magnitude increases significantly, accompanying the chain unfolding, when  $E > E_{II}^*$ . We study the condensed ion distributions modified by electric fields and discuss the connection of the modification with the change of chain morphology and mobility. Finally,  $E^*$  is studied by varying the chain length  $N$ . The inflection point is used as a third estimator  $E_{III}^*$ .  $E_{III}^*$  scales as  $N^{-0.63(4)}$  and  $N^{-0.76(2)}$  at  $C_s = 0.0$  and  $C_s^*$ , respectively.  $E_{II}^*$  follows a similar scaling law to  $E_{III}^*$  but a crossover appears at  $C_s = C_s^*$  when  $N$  is small. The  $E_I^*$  estimator fails to predict the critical field, which is due to oversimplifying the critical polarization energy to the thermal energy. Our results provide valuable information to understand the electrokinetics of PE solutions at the molecular level and could be helpful in micro/nano-fluidics applications.

PACS numbers:

---

\*Corresponding author. Email: pyhsiao@ess.nthu.edu.tw

## I. INTRODUCTION

Electric field-driven molecular analysis and sorting techniques have been widely used in many domains of research, such as chemistry, biology, and medical engineering. While the functionality of a bio-sensing or diagnostic system becomes more and more complicated and specialized today, electrokinetics remains the mechanism of choice for fluid actuation and manipulation at micrometer or submicrometer scales through the use of electric fields [1]. Therefore, a solid understanding of the electrokinetic behavior of ions, molecules, and macromolecules under the influence of electric fields is necessary to successfully integrate electric fields in micro/nano-fluidic devices.

Electrophoresis has been developed to separate charged macromolecules, such as DNA molecules or proteins, based upon their molecular weight for many years [2–4]. In most situations, electrophoresis is performed in sieving mediums such as gels. This is because, in free solutions, DNA molecules cannot be size-separated owing to the free-draining effect: the hydrodynamic friction and the molecular charge of a DNA molecule are both linearly proportional to the chain length. Hence, the electrophoretic mobility is length independent [5]. This phenomenon applies not only to DNA molecules but to any charged macromolecule, or polyelectrolyte (PE). In gels, the mechanism of electrophoretic separation is dominated by biased reptation of PEs and so the mobility has chain-length dependence [3, 6]. One drawback of the method is its low efficiency. Researchers continue to search for new techniques to separate charged molecules more efficiently [5], particularly in micro/nano-fluidics.

Recently, Netz proposed an idea to separate PEs electrophoretically in free solutions [7, 8]. PEs are polarized by electric fields and, if the electric field is strong enough, the polarization can induce chain unfolding, which renders a drastic increase in the electrophoretic mobility of the chains. Most importantly, the critical electric field to unfold chains is found to depend on the length. This dependence provides a plausible manner to separate chains by size in free solutions through an unfolding transition. If the idea could be applied in micro/nano-fluidics, the efficiency to separate DNA or other biomacromolecules by size could be improved. In Netz' idea-demonstrating work [7, 8], PEs were simply collapsed by monovalent counterions by setting a strong Coulomb coupling parameter between charged particles. However, this situation is not realistic because the PEs are usually collapsed by adding condensing agents such as multivalent salt [9]. Coulomb coupling is not as strong as in the simulation work

and furthermore, there are several species of counterions present in solutions which compete with each other to condense on the chains. The distributions of these ions play a crucial role in determining how PEs unfold in electric fields. Simulating polarization induced unfolding in salty solutions requires that individual ions be explicitly modeled with interactions that realistically account for aqueous conditions. This is what we will focus on in this study.

When salt is added in solutions, especially multivalent salt, PEs show complicated behavior [10–12]. The addition of multivalent salt can induce collapse or aggregation of chains, which causes phase separation. An excessive addition of multivalent salt can even cause the separated phases to dissolve back to a homogeneous solution; the collapsed and aggregated chains reexpand and separate from each other. Using these phenomena, researchers are able to control the dimension of DNA molecules in solutions and collapse them into small, very ordered toroidal particles [13]. In addition to the size control, the presence of multivalent counterions can also modify the charge distribution around PE chains [14] and lead to a specific phenomenon called “overcharging”, where the condensed counterions overcompensate the charge on chain surfaces [11, 15]. The total chain charge is also effectively altered. In certain conditions, the effective chain charge changes sign, a phenomenon called “charge inversion” [12]. A simple way to determine the effective charge is to study electrophoresis of PEs in weak electric fields [16]. Controlling the charge of PE-ion complexes is an important issue for gene therapy because it is related to the efficiency of DNA up-take by cells through endocytosis pathways [17].

In strong electric fields, the behavior of PEs becomes even more complicated because the charged particles in the complexes respond to the field in different ways, depending on the charge and the sign. Moreover, strong electric fields can change the molecular conformation in ways that are difficult to predict. The electrokinetics of the system is significantly modified. It has been demonstrated that DNA molecules condensed by polyvalent counterions such as spermine can be decondensed in DC electric fields if the electric field strength exceeds a threshold  $E^*$  [18]. Netz predicted that  $E^*$  should scale as  $N^{-3\nu/2}$  where  $N$  is the chain length and  $\nu$  is the Flory exponent [7, 8]. Simulations did observe scaling behavior but the scaling exponent measured did not agree with the prediction [19–21]. Hsiao and Wu considered a coiled chain as an ellipsoidal object of volume  $V$  and proposed a modification of the scaling law to be  $E^* \sim V^{-3/2}$  [19]. The salt valency dependence of  $E^*$  has also been explored [19–21]. The results show that the magnitude of electrophoretic mobility of chain

increases significantly above a chain unfolding transition, providing the foundation for chain separation in free solutions. Moreover, the chains can be unfolded to an elongated structure, which can then be utilized in the techniques of single-DNA molecule sequencing to increase spatial resolution of detection [22–24].

The response of PEs to alternating-current (AC) electric fields has also been investigated recently by simulations [21, 25]. Liu et al. found that chains are stretched and the sizes breath with the frequency of applied AC field only when the field strength exceeds some critical value and the frequency is smaller than the intrinsic relaxation frequency of the chain [21]. The work by Hsiao et al. further connected the critical AC field strength with the DC one, and the critical AC frequency with the inverse DC chain-fluctuation time [25]. A model, based upon Maxwell-Wagner dielectric theory, has also been developed, which explains the critical field-frequency correlation for chain unfolding in AC fields [25]. Recently, the conformational transition to a stretched state in AC fields has been experimentally demonstrated [26]. The chain size shows interesting hysteretic behavior upon sweeping the AC frequency. To understand the behavior, it is very important to first investigate chain conformations, ion distributions, and also the mobilities of the chains and ions in DC fields, because DC fields can be regarded as AC fields with zero frequency.

PE solutions involve both polymeric and electrolyte degrees of freedom, which brings many difficulties in dealing with these systems theoretically. Molecular dynamics simulations are a simple and economic tool, able to study systems in a controllable way and capture detailed information at the molecular level. Many simulation works investigate the structure of PEs in different solution conditions [10, 14, 27–30] and the response to electric fields [7, 8, 16, 19, 20, 25, 31, 32]. However, detailed information about the electrokinetics of different species of ions around the chains is lacking. Since the conformation of chains depends strongly on the concentration of salt in solutions, it is very important to understand the distribution of ions around the chains and see how these ions are affected by external electric fields. Therefore, in this study we aim to investigate electrophoresis of single PEs in multivalent salt solutions by means of molecular dynamics simulations. The rest of the paper is organized as follows. We explain the model and simulation setup in Sec. II. The results and discussions are presented in Sec. III. The effect of tetravalent salt concentration on chain conformation is discussed first (Sec. III-A). We then study polarization and determine the critical electric field at various salt concentrations (Sec. III-B). The electrophoretic mobility

of chains and condensed ions are investigated in Sec. III-C. The distribution of condensed ions and the effective charge of chains are presented in Sec. III-D and Sec. III-E. Finally, the mobility dependence on chain length is studied in Sec. III-F. We give our conclusions in Sec. IV.

## II. MODEL AND SIMULATION METHOD

Our system comprises a single linear chain, modeled by a bead-spring chain model. The chain consists of  $N$  monomer beads. Each bead carries a negative unit charge  $-e$  and dissociates one monovalent cation (or “counterion”) into the solution. The bonds connecting two adjacent monomers are modeled by the finitely extensible nonlinear elastic (FENE) potential

$$U_{\text{FENE}}(b) = -\frac{1}{2}kb_{\text{max}}^2 \ln \left( 1 - \left( \frac{b^2}{b_{\text{max}}^2} \right) \right) \quad (1)$$

where  $b$  is the bond length,  $b_{\text{max}}$  is the maximum extension, and  $k$  is the spring constant. Salt is added into the system. The salt molecules dissociate into tetravalent cations (also called “counterions”) and monovalent anions (“coions”) in the solution. All the particles — including the monomers, counterions, and coions — are modeled explicitly as spheres that are described by the purely repulsive Lennard-Jones (LJ) potential

$$U_{\text{LJ}}(r) = \begin{cases} 4\varepsilon_{\text{LJ}} \left[ \left( \frac{\sigma}{r} \right)^{12} - \left( \frac{\sigma}{r} \right)^6 + \frac{1}{4} \right] & , \text{ for } r \leq \sqrt[6]{2}\sigma \\ 0 & , \text{ for } r > \sqrt[6]{2}\sigma \end{cases} \quad (2)$$

where  $r$  is the separation distance;  $\sigma$  and  $\varepsilon_{\text{LJ}}$  represent the diameter and the hardness of the LJ sphere, respectively. Since the interaction between monomers is purely repulsive, our system corresponds to a good solvent. Charged particles also interact with each other via the Coulomb interaction

$$U_{\text{C}}(r) = k_{\text{B}}T\lambda_{\text{B}} \frac{Z_i Z_j}{r} \quad (3)$$

where  $T$  is the temperature,  $k_{\text{B}}$  is the Boltzmann constant, and  $Z_i$  is the charge valency of the  $i$ th particle.  $\lambda_{\text{B}} = e^2/(4\pi\epsilon_0\epsilon_r k_{\text{B}}T)$  is the Bjerrum length where  $\epsilon_0$  is the vacuum permittivity and  $\epsilon_r$  is the relative dielectric constant of the solvent. At the separation distance  $r = \lambda_{\text{B}}$ , the electrostatic energy between two unit charges is exactly the thermal energy  $k_{\text{B}}T$ . The solvent molecules are not modeled explicitly in the study. However, their effects are incorporated implicitly through the following three ways: (1) the dielectric constant  $\epsilon_r$ , which takes into

account of the dielectric screening of charge in the solvent medium, (2) the friction force  $-m_i\zeta_i\vec{v}_i$ , which models the drag acting on particle  $i$ , proportional to the moving velocity, (3) the stochastic force  $\vec{\eta}_i(t)$ , which simulates the thermal collisions of solvent molecules on the particle  $i$ . The equation of motion is the Langevin equation,

$$m_i\ddot{\vec{r}}_i = -m_i\zeta_i\dot{\vec{r}}_i + \vec{F}_c + Z_ieE\hat{x} + \vec{\eta}_i \quad (4)$$

where  $m_i$  is the particle mass,  $\zeta_i$  is the friction coefficient, and  $\vec{F}_c = -\partial U/\partial\vec{r}_i$  is the conservative force. In Langevin dynamics, the temperature is determined by the fluctuation-dissipation theorem:  $\langle\vec{\eta}_i(t)\cdot\vec{\eta}_j(t')\rangle = 6k_B T m_i\zeta_i\delta_{ij}\delta(t-t')$ . The external electric field is uniform and exerts an electric force  $Z_ieE\hat{x}$  on the particle  $i$  in the  $x$ -direction. The system is placed in a periodic rectangular box. Particle-particle particle-mesh Ewald sum is used to calculate the Coulomb interaction [33].

We assume that all the particles have the identical mass  $m$  and LJ parameters  $\sigma$  and  $\varepsilon_{LJ}$ . We set  $\varepsilon_{LJ} = 0.8333k_B T$ ,  $k = 5.8333k_B T/\sigma^2$ ,  $b_{\max} = 2\sigma$ ,  $\lambda_B = 3\sigma$ , and  $\zeta_i = 1\tau^{-1}$ , where  $\tau = \sigma\sqrt{m/(k_B T)}$  is the time unit. The chain length  $N$  is varied and the monomer concentration  $C_m$  is fixed at  $0.0003\sigma^{-3}$ , which describes a dilute polymer solution [34]. The simulation box is adjusted linearly with  $N$  in  $x$ -direction, and has a volume of  $1.3N \times 50.64 \times 50.64$ . This prevents chains from self-overlapping through the periodic boundary condition. The salt concentration  $C_s$  is varied from  $C_s = 0$  to  $C_s = 0.0006\sigma^{-3}$ , a range for the chain to exhibit the behavior of reentrant condensation [28–30]. The electric field strength  $E$  is varied over a wide range, from  $E = 0$  to  $2k_B T/(e\sigma)$ , to study its effect on the properties of the PE system. The Langevin equation is integrated by the Verlet algorithm. The integration time step  $\Delta t$  is equal to  $0.005\tau$  [35]. A pre-run phase takes about  $10^7$  time steps to bring the system into a stationary state, followed by a production-run phase of  $10^8$  time steps to cumulate data for analysis. Since hydrodynamic interaction is largely screened out under a typical electrophoretic condition [3, 36–38], we neglect the hydrodynamic interaction in this study. Recent simulations have demonstrated the validity of this approximation when the chain length is not short ( $N > 20$ ) [39]. We study the electrophoretic properties of chains at a fixed chain length  $N = 48$  for the first 5 subsections of Sec. III whereas in Sec. III.F,  $N$  is varied from 12 to 768. To simplify the notation, the value of a physical quantity will be reported in the  $(\sigma, m, k_B T, e)$ -unit system in the rest of the text. For example, the strength of electric field is described in units of  $k_B T/(e\sigma)$ , the dipole moment is in units of  $e\sigma$ , and

the electrophoretic mobility is in units of  $e\sigma^2/(\tau k_B T)$ , and so on.

### III. RESULTS AND DISCUSSIONS

#### A. Chain conformation in electric fields

In this section, we study the conformation of PEs at different salt concentrations  $C_s$  under the action of electric fields. The chain length  $N$  is 48. We first calculated the mean square radius of gyration  $R_g^2$ , which is used to characterize the chain size. The definition is given by  $R_g^2 = \sum_{i=1}^N \langle (\vec{r}_i - \vec{r}_{cm})^2 \rangle / N$  where  $\vec{r}_i$  is the position vector of the monomer  $i$  and  $\vec{r}_{cm}$  is the center of mass of the chain. The results are plotted in Fig. 1. Each curve shows how  $R_g^2$  varies with  $C_s$  at a given field strength  $E$ .

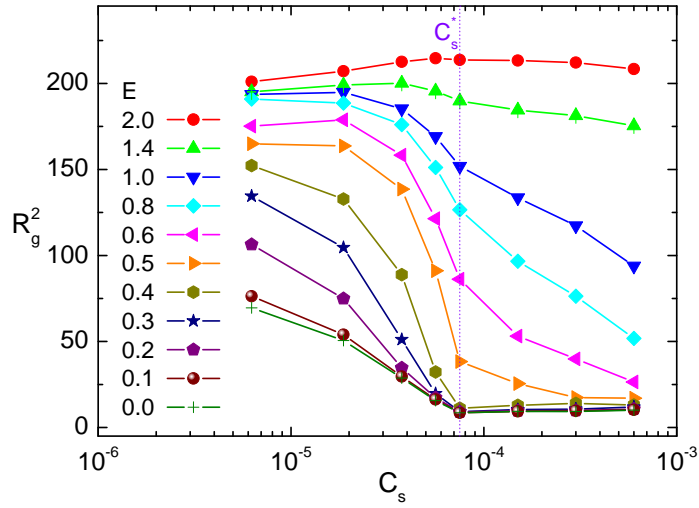


FIG. 1: Mean square radius of gyration  $R_g^2$  as a function of tetravalent salt concentration  $C_s$  at different strength  $E$  of electric field. The value of  $E$  can be read in the figure. The error bar of data in this paper is smaller than the size of data symbol if it is not presented.

We see that in zero electric field,  $R_g^2$  decreases with  $C_s$  up to the salt concentration  $C_s^* = 7.5 \times 10^{-5}$ . The value of  $C_s^*$  is one fourth of  $C_m$ , at which the amount of tetravalent cations in the solution are in charge equivalence with the monomers on the chain. The decrease of  $R_g^2$  shows that the chain collapses, which is due to ionic screening and to the bridging effect induced by the added tetravalent salt. At  $C_s = C_s^*$ , the chain is nearly neutralized by the condensation of tetravalent counterions. In the region  $C_s > C_s^*$ ,  $R_g^2$

becomes an increasing function of  $C_s$ . The chain size reexpands slightly. The collapse and the reexpansion of the chains can be regarded as a single-chain version of the PE precipitation and redissolution. These phenomena are collectively called “reentrant condensation” [15]. Reentrant condensation for PEs has been investigated in detail in theories [11, 15, 40–42], experiments [43, 44], and simulations [27–30].

Now let us focus on the cases in which the electric field is applied. All these curves lie above the zero-field limit. This result demonstrates that the chain is elongated by the applied electric field and therefore, takes a larger value of  $R_g^2$ . The stronger the electric field, the larger the deviation from the zero-field limit. However, this deviation also depends on  $C_s$ . While increased with  $E$  at a given  $C_s$  in the region  $C_s < C_s^*$ ,  $R_g^2$  is basically unchanged with  $E$  in the region  $C_s > C_s^*$  for  $E < 0.4$ . When  $E > 0.5$ , the PEs no longer exhibits a compact structure at  $C_s^*$ . The chain size continues to shrink with  $C_s$  for  $C_s > C_s^*$ . This shrinkage suggests that the excess of the tetravalent counterions in the solution helps the chains to collapse, against the action of the electric fields. In a very strong field such as  $E = 2.0$ ,  $R_g^2$  becomes basically a constant with  $C_s$ . The chain collapse by tetravalent salts is completely suppressed by the strong electric field.

We next calculated the asphericity  $A$  of the chain in electric fields. The quantity describes the degree of geometrical deformation away from a sphere and can be used to characterize the chain conformation. It is defined by  $A = \frac{1}{2} \langle ((\lambda_1 - \lambda_2)^2 + (\lambda_2 - \lambda_3)^2 + (\lambda_3 - \lambda_1)^2) / (\lambda_1 + \lambda_2 + \lambda_3)^2 \rangle$  where  $\lambda_1$ ,  $\lambda_2$ , and  $\lambda_3$  are the three eigenvalues of the gyration tensor of the chain. The tensor was calculated by  $\mathcal{T}_{\alpha\beta} = \sum_{i=1}^N (\vec{r}_i - \vec{r}_{cm})_\alpha (\vec{r}_i - \vec{r}_{cm})_\beta / N$ , where the subscripts  $\alpha$  and  $\beta$  denote one of the three Cartesian components  $x$ ,  $y$ ,  $z$  of the subscribed vector, respectively. The value of  $A$  ranges from 0 to 1. It is 0 for a perfect sphere and 1 for a rod. For a random coiled chain,  $A$  takes the value 0.431 obtained by simulations [45]. The left panel of Fig. 2 presents the asphericity  $A$  of our chain as a function of the electric field  $E$ . Each curve denotes one case running at a given  $C_s$ .

The curves are horizontal lines when  $E$  is small, showing that chain distortion does not happen in the weak electric fields. At  $C_s = 0.0$ , the value of  $A$  is 0.68. It is larger than 0.431, showing that the chain expands more than a coil does. We found that  $A$  decreases with  $C_s$  in this weak  $E$ -region, and reaches a minimal value 0.20 at  $C_s = C_s^*$ . The small value of  $A$  shows the formation of a compact globule structure. When  $C_s > C_s^*$ ,  $A$  begins



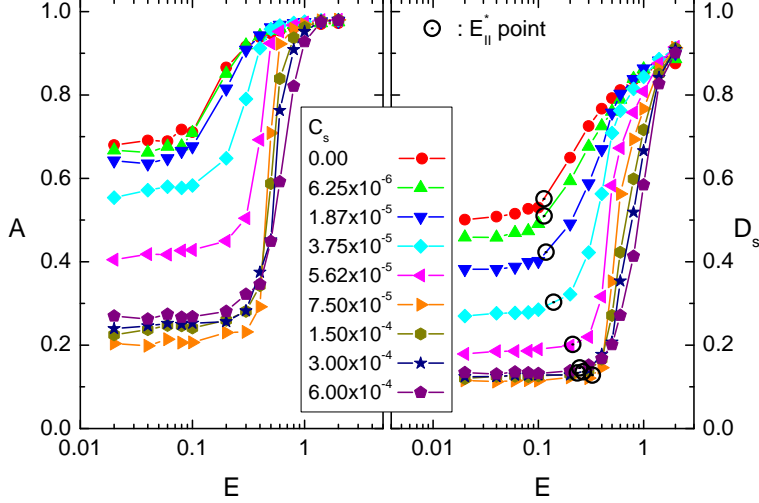


FIG. 2: Asphericity  $A$  and degree of chain unfolding  $D_s$  vs. electric field strength  $E$  at different  $C_s$ . The value of  $C_s$  is indicated in the legend. The symbol “ $\odot$ ” in the right panel denotes the threshold electrical field (denoted by  $E_{II}^*$  in the next section) at a given  $C_s$ .

to increase with  $C_s$ . The result demonstrates a chain reexpansion. In the intermediate  $E$  region between 0.1 and 1.0,  $A$  exhibits a drastic increase, showing the deformation of the chain by the electric field. At large field  $E = 2.0$ , the value of  $A$  is around 1. Therefore, the chain is deformed from its “natural” conformation in the zero field to a rodlike structure.

In the right panel of Fig. 2, we show the degree of chain unfolding  $D_s$  as a function of  $E$  at different  $C_s$ . Here  $D_s$  is defined to be the ratio of the chain end-to-end distance  $R_e$  to the chain contour length  $L_c$ . Similar to  $A$ ,  $D_s$  displays a sigmoidal increase when electric field is above some threshold value. In very high electric fields, the value of  $D_s$  can be as large as 0.9, showing that the chain is quasi-fully stretched. We estimate the threshold field by the onset point, at which  $D_s$  increases 10% from its zero-field limit. The dependence of the threshold field on  $C_s$  can be clearly seen in the figure.

To support the results of our calculation, we present in Fig. 3, Panel (a), (b), and (c), the snapshots of simulation at three salt concentrations  $C_s = 0$ ,  $7.5 \times 10^{-5}$ , and  $6.0 \times 10^{-4}$ , respectively. The three  $C_s$  present the three cases with the amount of the adding salt smaller than, equal to, and larger than the equivalence point  $C_s^*$ .

The left picture in each panel of the figure shows the case subjected to a weak electric field  $E = 0.02$ , which is below the critical field  $E^*$ . We can see that the chain exhibits an expanded-coil structure in the salt-free solution (Panel (a)), a compact globule structure at

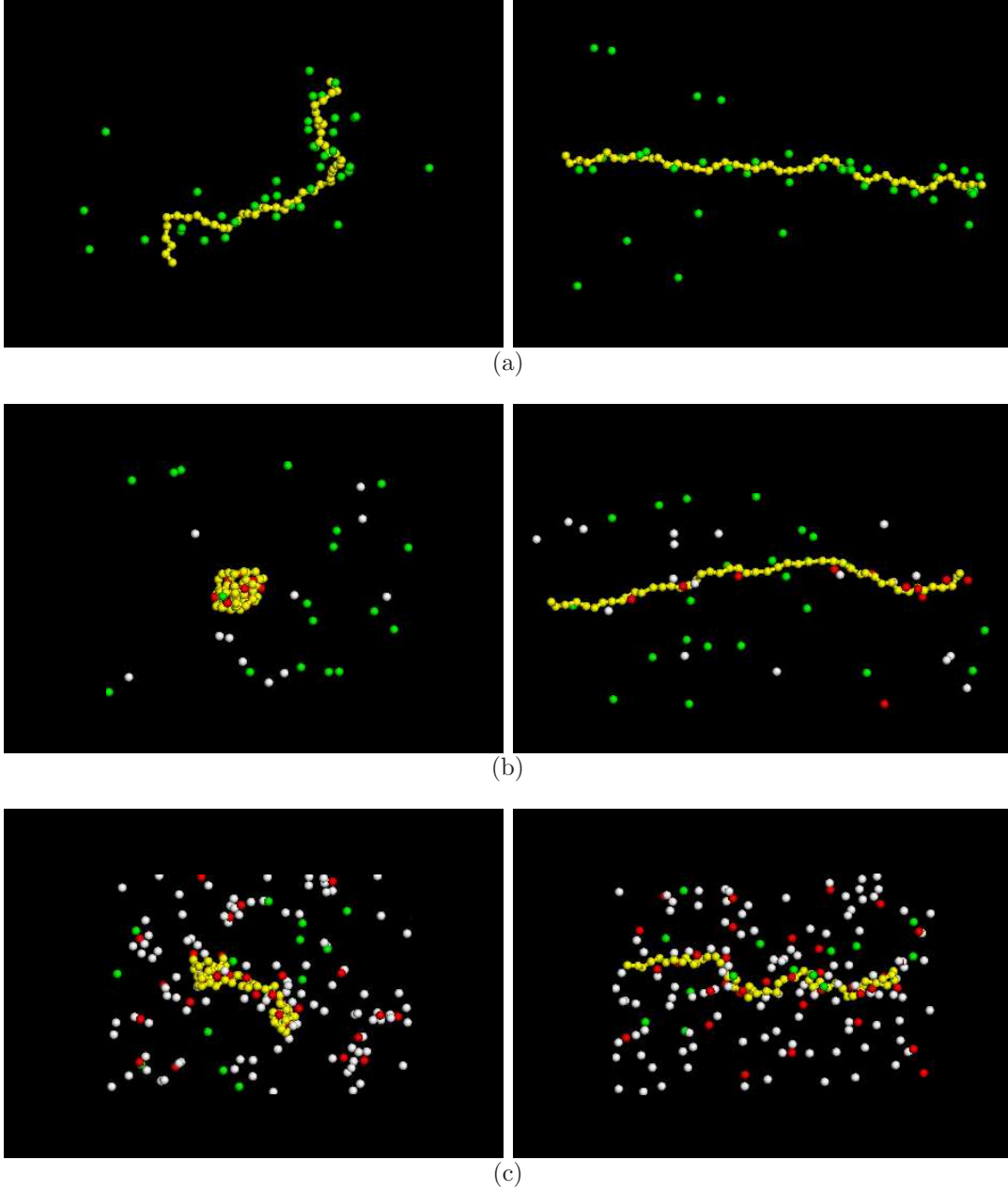


FIG. 3: (Color online) Snapshots of simulation at (a)  $C_s = 0.0$ , (b)  $C_s = 7.5 \times 10^{-5}$ , and (c)  $C_s = 6.0 \times 10^{-4}$ . In each panel, two pictures are presented: the left one is the case in a weak field  $E = 0.02$  and the right one is in a strong field  $E = 1.0$ . The PE is presented by a yellow bead-spring chain. The monovalent counterions, the tetravalent counterions, and the monovalent coions are presented by green-colored, red-colored, and white-colored spheres. The direction of electric field points toward the right direction.

the equivalence point (Panel (b)), and a less compact structure at the high salt concentration (Panel (c)), consistent with the calculations of the asphericity in Fig. 2. The right picture in each panel presents the case in the strong electric field  $E = 1.0$ , which is above  $E^*$ . We can see that the chain unfolds to an elongated structure. The chain size in Panel (a) is longer than in Panel (b), and than in Panel (c), which agrees with the results in Fig. 1 where  $R_g^2$  is a decreasing function over  $C_s$  for  $E = 1.0$ . Moreover, we can see that the elongated chain is aligned parallel to the field direction and the condensed monovalent counterions (in Panel (a)) and the condensed tetravalent counterions (in Panels (b) and (c)) cumulate more densely near the chain end which follows the field direction (the right-hand end in Fig. 3 figure). It shows that the chain is polarized in the electric field and possesses a dipole moment pointing to the field direction to reduce the system energy.

This dipole moment is precisely what causes the chain to unfold. The electric field causes an inhomogeneous distribution of counterions to condense on the chain. Due to this inhomogeneity, the electric force acting on the two sides of the chain is not balanced, which gives an effective tension along the chain. The chain is unfolded if this tension is strong enough to break the electrostatic binding between monomers by the condensed counterions.

## B. Polarization and critical electric field

The previous section discussed the existence of a critical field  $E^*$ , beyond which a PE is aligned along the field direction and drastically unfolded. To understand the unfolding mechanism in details, consider the polarization of a chain of polymerization  $N = 48$  in electric fields.

The energy of the electric field stored in a dielectric material is  $W = (1/2) \int \vec{D} \cdot \vec{E} dV$  where  $\vec{D}$  is the electric displacement field. Since  $\vec{D} = \epsilon_0 \vec{E} + \vec{P}$  where  $\vec{P}$  is the polarization density, the energy  $W$  can be written as a sum of two terms: the first is  $W_0 = (1/2) \int \epsilon_0 |\vec{E}|^2 dV$ , which represents the field energy in vacuum, and the second is  $W_{pol} = (1/2) \int \vec{P} \cdot \vec{E}$ , which denotes the polarization energy. In our study, the polarization energy is calculated by  $W_{pol} = \vec{p} \cdot \vec{E} / 2$  where  $\vec{p}$  is the induced dipole moment of the PE-ion complex. For an unfolding event to occur, the polarization energy  $W_{pol}$  is larger than the thermal fluctuation energy  $k_B T$ ,

according to Netz [7, 8]. The dipole moment of the PE complex can be calculated by

$$\vec{p} = \sum_{i \in \text{PE-complex}} Z_i e (\vec{r}_i - \vec{r}_{cm}) \quad (5)$$

where  $\vec{r}_i$  is the position vector of the  $i$ th particle and  $i$  runs over the entire PE complex (both the monomers and the condensed ions), and  $\vec{r}_{cm}$  is the center of mass of the entire complex. There exists no definite way to define a PE complex. In this study, we primitively define the PE complex by a constant threshold distance  $r_t$ : a PE complex comprises the chain itself and the ions with the distance to the chain smaller than  $r_t$ . These ions are said to condense on the chain. We chose  $r_t = \lambda_B$ . This criterion has been used previously to study ion condensation on a rigid chain [46] but other definitions can be used [39]. Since the polarization will occur in the field direction, we calculated here the  $x$ -component of the dipole moment,  $p_x$ . The results are presented in Fig. 4 as a function of  $E$  for different  $C_s$ . The criterion for chain unfolding is that  $p_x \geq 2k_B T/E$ , and a dashed line demarcates the boundary of the two regions in the figure.  $W_{pol}$  is larger than  $k_B T$  above the line, whereas smaller below the line.

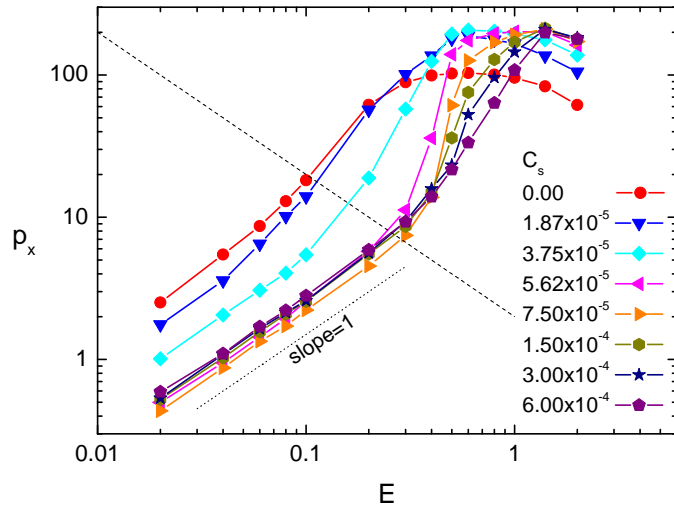


FIG. 4: Dipole moment  $p_x$  as a function of  $E$ . Each curve corresponds to a salt concentration whose value can be read in the figure. The dashed line is the equation  $p_x = 2k_B T/E^*$  and the dotted line is a reference line with the slope equal to 1.

The points of  $p_x$  fall on a straight line in the log-log plot in the weak field region  $E < 2k_B T/p_x$ . The slope of the line is 1, which follows exactly linear response theory,  $p_x = \alpha E$ . The polarizability  $\alpha$  is directly related to the height of the line in the figure.  $\alpha$  takes a large

value for a non-collapsed chain, and is smallest for a collapsed chain at  $C_s = C_s^*$ . In the field region above the dashed line,  $p_x$  deviates from this simple power law. Approximately above the dashed line, the curves grow faster than the linear dependence but then curve down, exhibiting a hook-like behavior.

In the weak field region, the chain conformation is not perturbed by the applied electric field. However, the displacement of the condensed ions on the chain is still possible. It is hence the ion displacement that is responsible for the formation of the dipole moment and results in the linear response behavior. When the electric field is strong enough to unfold the chain, the chain elongation provides the further possibility for the condensed ions to migrate on the chain [25]. Consequently, the dipole moment acquires a value larger than predicted by linear response theory. In very strong electric fields, the chain reaches its maximum extension. Further elongation of the chain becomes impossible. Increasing the electric field can cause condensed ions on the chain to be stripped off. The number of the condensed ions decreases. As a consequence, the dipole moment decreases, resulting in the hook-like curve.

The critical electric field  $E^*$  is estimated as the intersection of the simulated  $p_x$  curves with the unfolding transition  $p_x = 2k_B T/E^*$ . The obtained critical field is reported in Fig. 5 as a function of  $C_s$  and denoted  $E_I^*$  (for reasons that will be clear momentarily). We can see

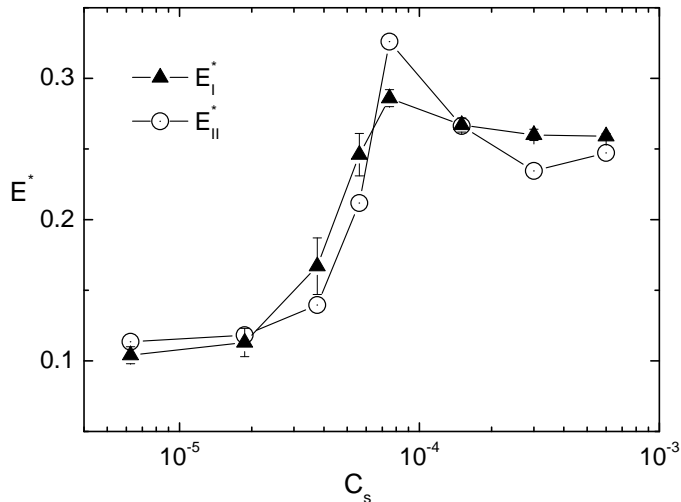


FIG. 5: Critical electric field  $E^*$  as a function of  $C_s$ .  $E^*$  is determined by two different methods:  $E_I^*$  from the polarization energy and  $E_{II}^*$  from the onset point of  $D_s$ .

that  $E_I^*$  increases with  $C_s$  and reaches the maximum value at  $C_s = C_s^*$ , and then, decreases slightly. This behavior is consistent with what we have observed in Fig. 1. The chain is

easier to stretch in the low-salt region ( $C_s < C_s^*$ ) than in the high-salt region ( $C_s > C_s^*$ ). To verify that the chain begins unfolding at  $E = E_I^*$ , the threshold field obtained from the onset increasing of  $D_s$  in Fig. 2 is plotted and denoted by  $E_{II}^*$ . The consistency between  $E_I^*$  and  $E_{II}^*$  data seems to suggest that chain unfolding occurs as when linear response theory no longer holds. Nonetheless, further verification through varying the chain length from  $N = 12$  to 768 shows that  $E_I^*$  is not always situated at the break-down of the linear dependence, as shown in Fig. 6.

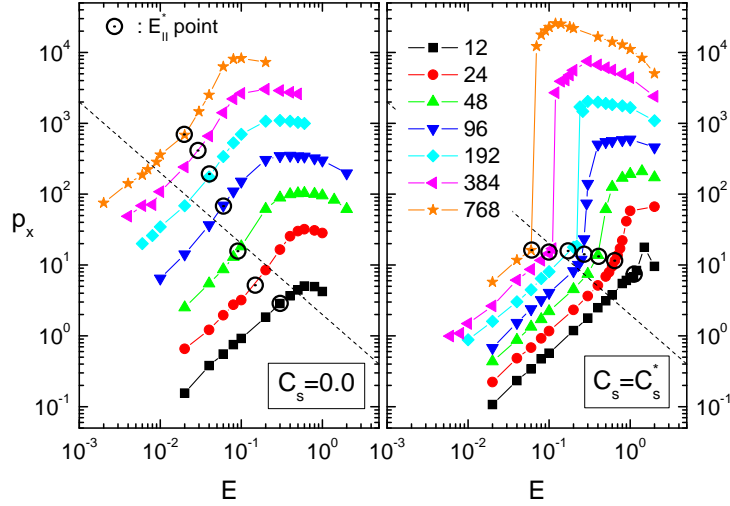


FIG. 6: Dipole moment  $p_x$  as a function of  $E$  at  $C_s = 0$  and  $C_s = C_s^*$ . Chain length  $N$  is indicated in the right panel. The dashed line defines the equation  $p_x = 2k_B T / E^*$ . The symbol “ $\odot$ ” denotes the dipole moment at  $E = E_{II}^*$ .

Indicating the onset-critical point on the curve, we clearly see that the dipole moment deviates from the linear behavior at  $E = E_{II}^*$ , but not at  $E = E_I^*$ . Therefore, the criterion  $W_{pol} \geq k_B T$  for chain unfolding is too simple to be precise. A real unfolding point can happen with the polarization energy larger or smaller than  $k_B T$ , depending on both the chain length and salt concentration. It necessitates a fundamental understanding of the unfolding mechanism in the future to set up a correct criterion for the problem. The results shown here demonstrate that chain unfolding is tightly connected with the polarization change.

### C. Electrophoretic mobility

We have seen that PE-ion complexes exhibit a drastic unfolding transition when the electric field is stronger than  $E^*$ . One pertinent question is whether the mobility of the chain shows a drastic change too, accompanying the conformational transition. Also, it is very important to know the mobility of ions, especially the condensed multivalent counterions, because these ions play a decisive role in determination of the chain conformations.

The mobility of the chain and of the condensed tetravalent counterions are defined as  $\mu_{pe} = v_{pe}/E$  and  $\mu_{+4}^c = v_{+4}^c/E$ , respectively, where  $v_{pe}$  and  $v_{+4}^c$  are, in turn, the velocities of the chain and the condensed tetravalent counterions in the field direction. The results are presented in Fig. 7, Panels (a) and (b), for  $\mu_{pe}$  and  $\mu_{+4}^c$ , respectively, as a function of  $E$  for different  $C_s$ . The sign of the obtained mobility can be positive or negative, denoting the moving direction of the studied object toward the  $+x$ - or the  $-x$ -direction. To investigate the relationship between the mobility change and the conformational transition, we have plotted on the curves of the data the corresponding critical field  $E^*$  (the  $E_{II}^*$ ) by the symbol “ $\odot$ ”.

We can see in Fig. 7(a) that when  $E < E^*$ ,  $\mu_{pe}$  is a constant and depends on the salt concentration. For  $C_s < C_s^*$ , the value of  $\mu_{pe}$  is smaller than zero because the effective chain charge is negative, the same sign as the bare chain charge. Increasing  $C_s$  leads to a decrease of  $|\mu_{pe}|$ . The absolute net chain charge decreases due to the condensation of the counterions on the chain backbone. At  $C_s = C_s^*$ ,  $\mu_{pe}$  is approximately zero. This is because the total charge of the tetravalent counterions in the solution is equivalent to the charge of the PE. The chain is effectively neutralized upon the condensation of these ions. If  $C_s$  is increased above  $C_s^*$ ,  $\mu_{pe}$  becomes positive. The chain now moves in the  $+x$ -direction and the effective charge of the PE-ion complex is positive. In other words, a charge inversion occurs. Charge inversion induced by multivalent salt has been observed in experiments [47]. Nonetheless, researchers continue to put their efforts on this study area for a full understanding of the underlying mechanism [16, 48, 49]. When the electric field is strong  $E > E^*$ ,  $\mu_{pe}$  is no longer a constant but monotonically decreases with  $E$ . The fact that the effective chain charge becomes more negative suggests that a strong electric field strips the condensed counterions off the chain. A detailed study concerning the number of the ions condensing on the chain will be presented in the next section. Our results reveal that charge inversion can

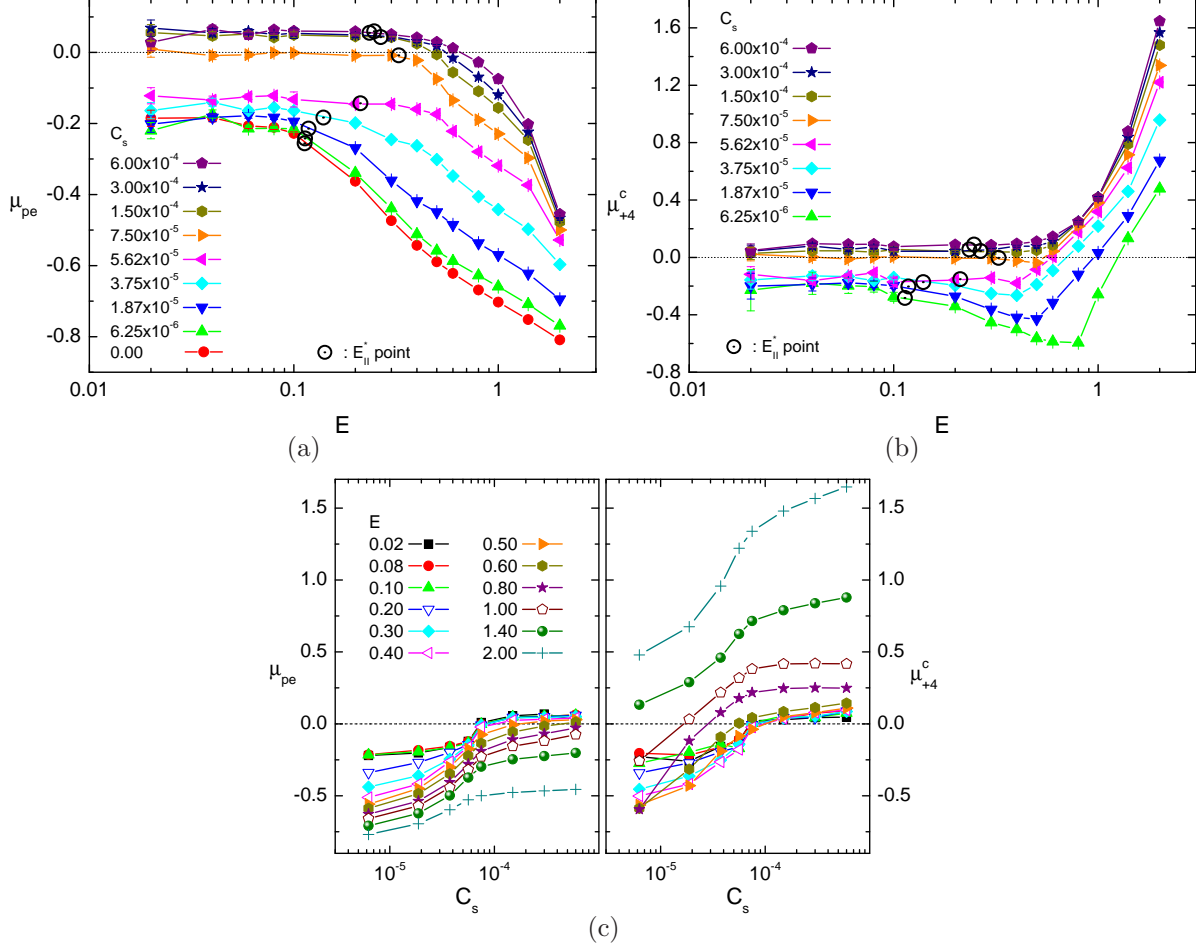


FIG. 7: Mobility of (a) chain  $\mu_{pe}$  and (b) the condensed tetravalent counterions  $\mu_{+4}^c$  as a function of  $E$ . Each curve denotes one case running at a specific  $C_s$ . The value of  $C_s$  can be read in the figure. The critical field  $E_{II}^*$  is indicated on the corresponding curve by the symbol “ $\odot$ ”. (c)  $\mu_{pe}$  and  $\mu_{+4}^c$  vs.  $C_s$  in different  $E$  fields, replotted from the data of (a) and (b). The value of  $E$  is indicated in the left panel.

be suppressed by strong electric fields. Comparing mobility with the conformational change demonstrates that chain mobility and unfolding are closely related.

Fig. 7(b) shows the mean mobility of the tetravalent counterions  $\mu_{+4}^c$  condensed on the chain. We observed that  $\mu_{+4}^c$  is approximately equal to  $\mu_{pe}$  when  $E$  is small. We recall that the mobility of tetravalent counterions is positive in a free solution, but Fig. 7(b) shows that  $\mu_{+4}^c < 0$  when  $C_s < C_s^*$ . A negative  $\mu_{+4}^c$  clearly demonstrates that the electrostatic interaction between tetravalent counterions and monomers sets a strong constraint on the ions. The ions are dragged along with the chain and consequently,  $\mu_{+4}^c \simeq \mu_{pe}$ . When  $E$



is strong enough to break the constraint,  $\mu_{+4}^c$  deviates from  $\mu_{pe}$ . In very strong electric fields, these ions glide along the chain surface in the  $+x$ -direction;  $\mu_{+4}^c$  thus takes a positive value. The mobility difference between the chains and the condensed ions suggests that ion condensation must take place in a dynamic way. The condensed ions glide on the chain and are eventually stripped off the chain end. The ions from the bulk solution continually condense onto the chain from the other end. The process repeats continuously and a balance is established.

Please notice that the field required to cause  $\mu_{+4}^c$  to deviate from  $\mu_{pe}$  is stronger than  $E^*$ . This suggests that the chain unfolding occurs before the ions are able to glide along the chain. Therefore, there is a field region in which the chain has unfolded but the condensed tetravalent counterions are too tightly bound to glide. Since  $\mu_{pe}$  becomes more and more negative, so does  $\mu_{+4}^c$  before shooting up in stronger  $E$  fields. Consequently, the  $\mu_{+4}^c$  curve exhibits a minimum. For  $C_s > C_s^*$ , the binding between condensed tetravalent counterions and monomers becomes effectively weaker because of overcharging (see Fig. 8(b)). The field region where the chain unfolds without ion gliding shrinks as  $C_s$  is increases. The minimum disappears and  $\mu_{+4}^c$  grows monotonically with  $E$ . Fig. 7(c) shows the mobility presented as a function of salt concentration in different field strength. As we can see,  $\mu_{pe}$  and  $\mu_{+4}^c$  both increase with  $C_s$ . Moreover,  $\mu_{pe}$  is roughly equal to  $\mu_{+4}^c$  over the studied  $C_s$  for  $E \leq 0.4$ . For  $E > 0.4$ , very different behavior is observed. The mobility of the tetravalent ions increases much faster than  $\mu_{pe}$ , and eventually becomes entirely positive at very strong  $E$  while  $\mu_{pe}$  remains negative.

We remark that in this study, each data point of the mobility is calculated under the action of an electric field at a given strength, once the system reaches a steady state. Figs. 7(a) and (b) are not obtained by sweeping the DC field strength at a constant rate. Therefore, no hysteresis is displayed. Our results report the mobilities in a stationary, pseudo-equilibrium condition. For simulations done by sweeping the field strength, one would expect the occurrence of a hysteretic behavior in mobility, and also in chain size, if the sweeping rate is fast. There exists two relevant characteristic times in chain conformational transitions: the first is the chain unfolding time to transition from a coiled or globular chain to an elongated one, and the other is the collapse time to relax from an elongated chain to a coil or globule. The unfolding time is generally longer than the collapse time because additional time is needed to disentangle a coiled or globular chain. The chain size (and therefore mobility) will follow

a different path when sweeping from a weak DC field to a strong one and then from a strong field to a weak one, presumed that the total sweeping time would be comparable to the two characteristic times. This deserves further investigation in the future. A counterpart has been shown in experiments studying chain-size hysteresis when AC field frequency is changed at a fixed field amplitude [26].

#### D. Number of condensed ions and effective chain charge in electric fields

In this section, we study the number of ions condensed on the chain ( $N = 48$ ) and effective chain charge in electric fields. As in the previous section, an ion is regarded to condense onto the chain if its distance to the chain is smaller than the threshold distance  $r_t = \lambda_B$ . Once the condensed ions are identified, the effective chain charge can be calculated by summing the charges of the condensed ions and the chain monomers. Since there are three types of ions in the simulation box, we treat each species independently. The results are presented in Fig. 8 as a function of  $E$  where  $N_{+1}^c$ ,  $N_{+4}^c$ , and  $N_{-1}^c$  are the numbers of the condensed monovalent counterions, tetravalent counterions, and coions, respectively. In order to make comparison with the chain conformational transition, we have plotted the chain asphericity  $A$  at three representative  $C_s$  in the figure.

We observe that  $N_{+1}^c$  is unperturbed by  $E$ , when  $E < E^*$ . This constant value decreases with  $C_s$  and goes to zero when  $C_s \geq C_s^*$ : There are no condensed monovalent counterions above the equivalence point. When  $E > E^*$ ,  $N_{+1}^c$  shows a decreasing behavior with  $E$  for  $C_s \leq 3.75 \times 10^{-5}$  but at  $C_s = 5.62 \times 10^{-5}$  and  $7.5 \times 10^{-5}$ , the  $N_{+1}^c$  exhibits a small hump. For even higher  $C_s$ , the curve increases slightly. By comparing with the chain asphericity, we find that these variations take place at the moment when the chain changes its conformation. Therefore, the number of condensed ions is closely related to chain morphology. How salt-induced chain conformation affects the ion condensation in zero electric field has been studied in reference [20].

$N_{+1}^c$  at  $C_s = 0.0$  can be used to verify Manning condensation theory [46]. The theory states that counterion condensation takes place on a rigid PE while the mean distance per unit charge on the chain is smaller than the Bjerrum length. It results in an effective chain charge equal to  $-eL_c/\lambda_B$ . In our simulations, the mean distance before condensation takes place is equal to the averaged bond length  $\langle b \rangle = 1.1$ . Hence Manning's theory predicts an

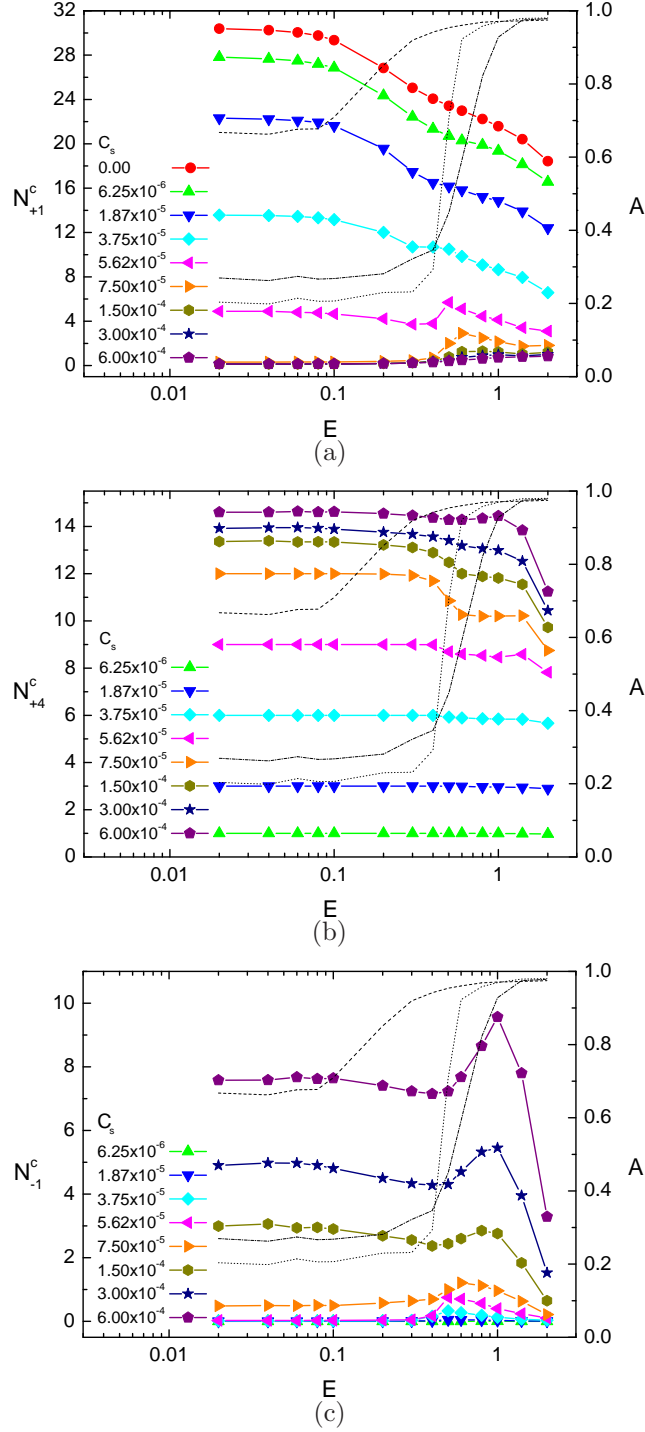


FIG. 8: Number of condensed (a) monovalent counterions  $N_{+1}^c$ , (b) tetravalent counterions  $N_{+4}^c$ , and (c) coions  $N_{-1}^c$  as a function of  $E$ . The salt concentration can be read in the figures. In each panel, the chain asphericity  $A$  at  $C_s = 6.25 \times 10^{-6}$  (dashed curve),  $7.5 \times 10^{-5}$  (dotted curve), and  $6.0 \times 10^{-4}$  (dash-dotted curve) are plotted to illustrate the chain conformational change. The value of  $A$  is read from the right y-axis of the plot.

effective chain charge of  $-17.3$ . This is equivalent to  $30.7$  monovalent counterions condensing on the chain. Our simulations obtained  $N_{+1}^c = 30.4$ , very close to the prediction, although the chain is flexible and of finite length, which does not follow the assumption of a rigid, infinitely long chain. This consistency shows that the theory is a good approximation of flexible chains and also that the choice for the condensation threshold  $r_t = \lambda_B$  able to capture the condensation phenomena.

In Fig. 8(b), we observed that  $N_{+4}^c$  remains constant for a much wider range of electric field than  $N_{+1}^c$ . For example, in  $C_s \leq 3.75 \times 10^{-5}$ , this number varies very little over the studied field strengths, although the electrophoretic mobility (in Fig. 7) does show some variation. Therefore, the decrease of  $\mu_{pe}$  in this salt region is directly related to the stripping-off of condensed monovalent counterions from the chain. Moreover, we observed that  $N_{+4}^c$  exhibits a two-step decrease at  $C_s \simeq C_s^*$ . By referring to the corresponding  $A$  curve, we can find that the first plateau appears in the weak field region where the chain exhibits a unperturbed, globular structure and the condensed tetravalent counterions are wrapped within the twisted chain [28, 29]. The second, small plateau occurs when  $E$  is strong and the chain is completely stretched with  $A \simeq 1$ . In this case, the number of the condensed tetravalent counterions maintains a constant that is smaller than the globular chain value. If the applied field is very strong, such as  $E > 1$ , the tetravalent counterions can be stripped off the chain violently; as a consequence,  $N_{+4}^c$  decreases. The two-step plateaus are smeared out when  $C_s$  is high. It is because a large number of the tetravalent counterions appears in the solution, obscuring the boundary between condensed and non-condensed ions.

Fig. 8(c) shows that in weak fields, there are nearly no coions condensed on the chain when  $C_s < C_s^*$ . In the high-salt region above the equivalence point  $C_s^*$ , the coion condensation significantly increases. This is because the effective charge becomes positive, manifested by the inversion of chain mobility as seen in Fig. 7(a), and so attracts the coions to the chain. After being constant in weak fields,  $N_{-1}^c$  decreases slightly with  $E$  but then displays a large peak in strong fields. The peak can be associated with the chain conformational transition because tetravalent counterions condensed on a stretched, elongated chain are more exposed to the bulk solution than ones condensed/wrapped in a unperturbed, coiled or globular chain and hence, attract more coions. The condensed coions constitute an outer layer of the PE complex. Therefore, once the chain is fully stretched, the increasing electric field can “blow” coions off due to the weak condensation, causing  $N_{-1}^c$  to decrease drastically.

The above results show that the ions do not condense on the chain in a universal way. Condensation depends strongly on the ion valency and the chain conformation in electric fields. The tetravalent counterions compete with the monovalent counterions. Therefore, while  $N_{+4}^c$  increases with  $C_s$ ,  $N_{+1}^c$  decreases. On the other hand, the coions collaborate with the tetravalent counterions;  $N_{-1}^c$  increases with  $C_s$  when  $C_s > C_s^*$ , following the trend of  $N_{+4}^c$ . The non-monotonic behavior of change can be seen in Fig. 9(a) where the total number of the condensed ions  $N_{ion}^c$  is plotted against  $E$  at different  $C_s$ . Nonetheless, the

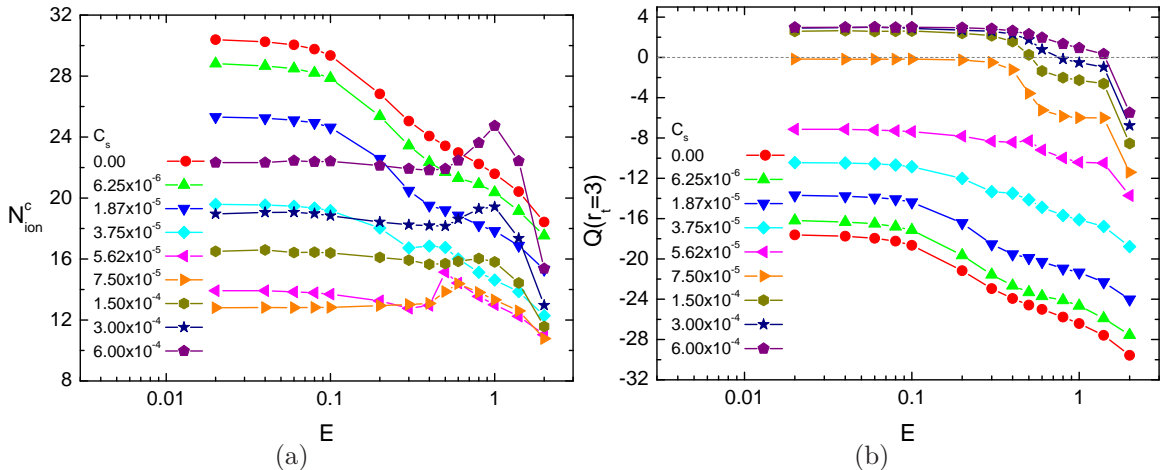


FIG. 9: (a) Total number of condensed ions  $N_{ion}^c$ , and (b) total charge of chain,  $Q(r_t = \lambda_B)$ , inside the condensation region  $r_t = \lambda_B$ , as a function of  $E$  at different  $C_s$ .

total charge inside the condensation region,  $Q(r_t = \lambda_B)$ , (presented in Fig. 9(b)) shows a more regular, decreasing behavior. We regarded  $Q(r_t = \lambda_B)$  as the effective charge and its variation compares well with the behavior of the chain mobility  $\mu_{pe}$  shown in Fig. 7(a). By comparing the results of Fig. 9(a) and (b), we conclude that it is not the number of ions but rather the total charge of the PE-ion complex that is constantly being reduced by the strong electric field.

### E. Ion distribution along the chain and the mobilities

As we have seen and studied, the PE-ion complex is polarized by an external electric field. The polarization results from both the migration of the ions condensed on the chain and the conformational change. In this subsection, we study how the ion distribution along the chain varies with the electric field and see how this distribution is related to the mobilities

of the chain and the condensed ions. We associate a condensed ion to the monomer with which it is closest, and calculated the mean number  $n$  of the condensed ions associated with each monomer. The monomers are indexed by  $i$  through the chain such that the increment of the index follows the sense of the field direction and not necessarily the position along the chain. A front end and a rear end of the chain are then defined to be the monomers with the smallest and the largest index, respectively. Thus,  $n(i)$  is the distribution function of the condensed ions. We study four representative cases of  $C_s$ .

The first case considers the salt-free solution. The only ions presented in this case are the monovalent counterions. Fig. 10(a) shows the number distribution of the condensed monovalent counterions on the chain,  $n_{+1}(i)$ .

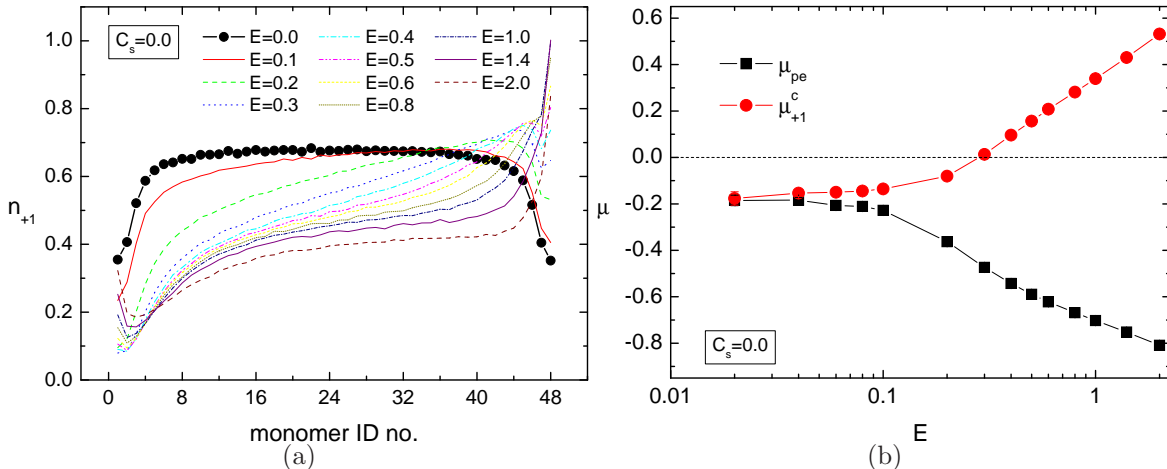


FIG. 10: (a) Distribution of condensed monovalent counterion along chain,  $n_{+1}(i)$ , at  $C_s = 0.0$  in different electric fields  $E$ . The value of  $E$  is indicated in the figure. (b) The mobility of the chain  $\mu_{pe}$ , and of the condensed monovalent counterions  $\mu_{+1}^c$ , as a function of  $E$ .

In the zero field limit, the  $n_{+1}$  curve is flat in the interior region of the chain and decreases near the two chain ends. The decrease can be attributed to the symmetry broken near the chain ends because there exists no monomer outside the ends and hence the attractive force to condense the counterions is weaker than in the interior. The whole distribution curve is symmetric with respect to the middle of the chain. The application of an electric field breaks this symmetry by tilting the distribution curve against the field direction, as shown. The condensed monovalent counterions accumulate near one end and are depleted near the other, leading to a polarization vector pointing in the field direction. The curve shifts downward as

$E$  increases. Since the area below the curve represents the number of ions condensed on the chain, the downward-shifting shows the decrease of the number of condensed counterions, which is consistent with the result in Fig. 8(a). The shape of  $n_{+1}$  evolves and becomes a tangential curve when  $E$  is very strong. In order to understand the kinetics of the condensed ions, we plot the mobility of the chain  $\mu_{pe}$  and the mobility of the condensed ions  $\mu_{+1}^c$  in Fig. 10(b). We found that  $\mu_{+1}^c$  is basically equal to  $\mu_{pe}$  in the weak fields, which shows that the condensed counterions reside statically on the chain.  $\mu_{+1}^c$  deviates significantly from  $\mu_{pe}$  when  $E$  goes beyond 0.1. This deviation shows that there is relative motion between the condensed monovalent counterions and the chain: The ions glide along the chain. Since the chain has finite length, the gliding means that the ions are dynamically, rather than statically, condensed on the chain. Once condensed onto the chain, an ion glides along the chain backbone and accumulates at the chain end. A condensed ion at the chain end must then leave the chain to maintain a steady number of the condensed ions.

For the second case, consider a salt concentration smaller than the equivalence point,  $C_s = 1.875 \times 10^{-5}$ . According to Fig. 8, there are nearly no coions condensing onto the chain. Therefore, we show only the distribution functions for the condensed monovalent counterions,  $n_{+1}(i)$ , and for the condensed tetravalent counterions,  $n_{+4}(i)$ . The results are presented in Figs. 11(a) and (b), respectively.

Observe that in the zero field limit, the  $n_{+1}(i)$  and  $n_{+4}(i)$  curves are both flat in the interior and symmetric to the middle of the chain. When an electric field is applied, the symmetry is broken.  $n_{+1}$  displays a large skewed peak in the interior region of the chain, while  $n_{+4}$  shows multiple peaks close to the rear end. The number of peaks in  $n_{+4}$  is 3 for  $0.2 \leq E \leq 0.5$ , which corresponds exactly to the number of the tetravalent counterions added at this salt concentration, *i.e.*, the tetravalent counterions completely condense. The distinct peaks reveals that the ions are localized on the chain, similar to a 1-dimensional crystal. This localization happens when appropriate strength of electric field is applied. If  $E$  is weak, the ions cannot be localized and the  $n_{+4}$  curve simply tilts. If  $E$  is strong, they are pushed forcibly to the rear end and only one peak is visible. Similar phenomena have been observed for other  $C_s < C_s^*$ . The peak of the  $n_{+1}$  curve appears right after the peaks of the  $n_{+4}$  curve. This non-overlapping of the two species results from mutual exclusion between the condensed monovalent counterions and tetravalent counterions due to their Coulomb repulsion. Since the external electric force exerted on an ion is proportional to

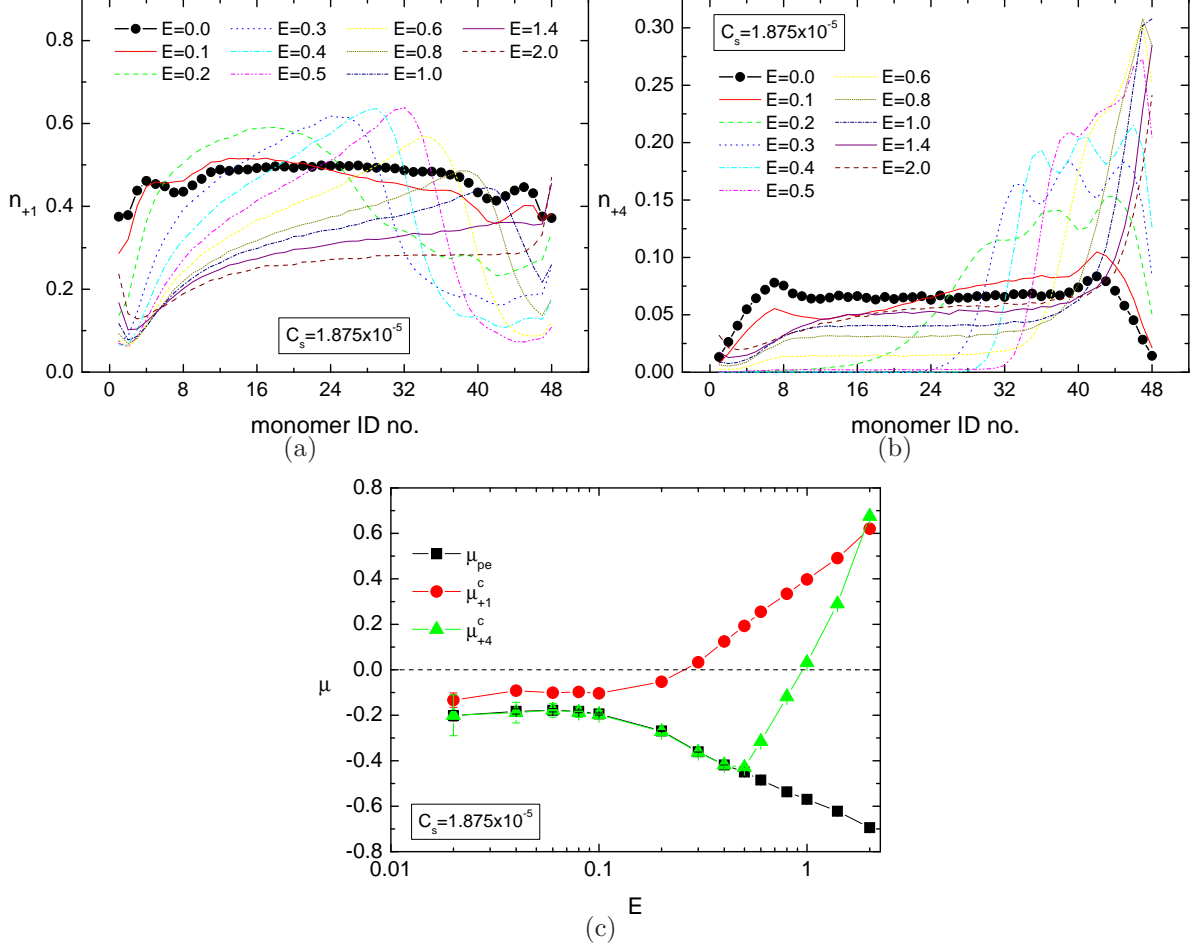


FIG. 11: (a) Distribution of condensed monovalent counterions on chain,  $n_{+1}(i)$ , at  $C_s = 1.875 \times 10^{-5} (< C_s^*)$  in different electric fields  $E$ . The value of  $E$  can be read in the figure. (b) Same as (a), but for condensed tetravalent counterions,  $n_{+4}(i)$ . (c) The mobility of the chain  $\mu_{pe}$ , of the condensed monovalent counterions  $\mu_{+1}^c$ , and of the condensed tetravalent counterions  $\mu_{+4}^c$ , as a function of  $E$ .

the ion valency, the tetravalent counterions are pushed more strongly by the electric fields and move closer to the chain end. The monovalent counterions suffer a weaker force and condense just behind the tetravalent counterions.

We also plot the mobility of the chain and the condensed ions as a function of  $E$  in Fig. 11(c) to study the kinetics of the system. We can see that the mobility of the tetravalent counterions  $\mu_{+4}^c$  coincides with  $\mu_{pe}$  in small fields and deviates from it when  $E > 0.5$ . The tight coincidence shows that the tetravalent counterions are tightly bound to the chain and move with it. The mobility of the condensed monovalent counterions  $\mu_{+1}^c$  also takes a value



close to  $\mu_{pe}$  when  $E \leq 0.1$  but not as close as when  $C_s = 0.0$  (cf. Fig. 10.) The tetravalent counterions repel the condensed monovalent counterions on the chain, which loosens the condensation. Recall that the deviation of  $\mu_{+4}^c$  from  $\mu_{pe}$  occurs around  $E = 0.5$ . This is about 4 times the field strength as when  $\mu_{+1}^c$  begins to deviate from  $\mu_{pe}$ . And the number 4 is equal to the valency ratio between the two species of the counterions, which can be explained by law of friction. Assume that the friction coefficient of the surface is effectively  $\xi$ . The criterion for a condensed ion to glide along the chain surface is governed by  $F_E \geq \xi F_n$ , where  $F_E = ZeE$ , and  $F_n$  is the force normal to the chain surface, which is estimated by  $k_B T \lambda_B Z^2 e^2 / \sigma^2$ . The square of  $Z$  appears in  $F_n$  because of the matching (or interaction) of a  $Z$ -valent counterion with  $Z$  monomers when it condenses on the chain. Therefore, the threshold electric field to glide a condensed counterion is approximately proportional to the valency.

The third case studies the system at the equivalence point  $C_s^*$ . At this salt concentration, no monovalent counterions or coions condense on the chain; so only the distribution function for the tetravalent counterions is shown. The results of  $n_{+4}(i)$  and the mobilities for the chain and the ions are presented as a function of  $E$  in Fig. 12.

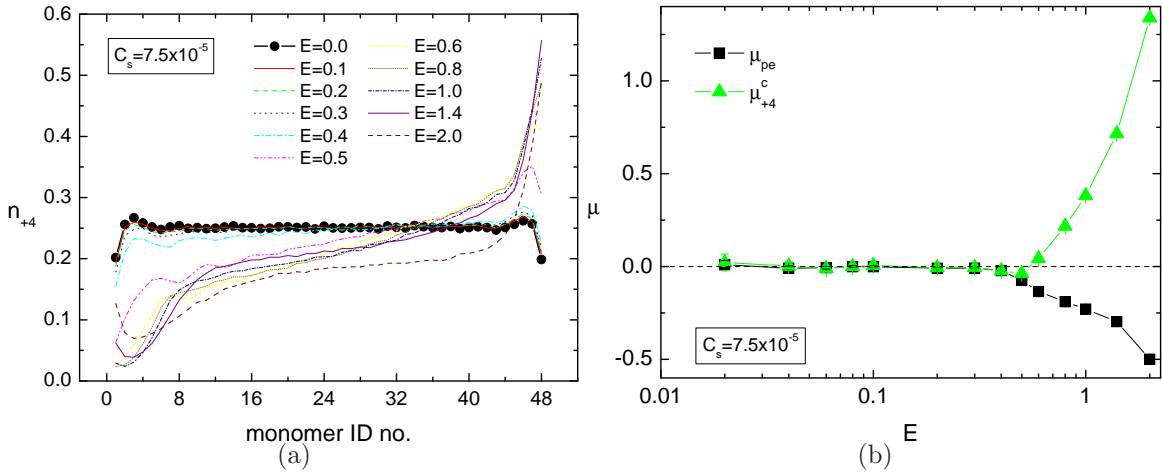


FIG. 12: (a) Distribution of condensed tetravalent counterions on chain at  $C_s = 7.5 \times 10^{-5} (= C_s^*)$  in different electric fields  $E$ . The value of  $E$  can be read in the figure. (b) The mobility of the chain  $\mu_{pe}$  and of the condensed tetravalent counterions  $\mu_{+4}^c$  as a function of  $E$ .

The behavior of  $n_{+4}(i)$  looks similar to  $n_{+1}(i)$  in Fig. 10(a). The curve tilts, shifts downward, and eventually shows a tangential distribution as  $E$  increases. Since the condensed

ions have large valency, the condensation is strong. The chain is charge-neutralized by the condensed ions and Fig. 12(b) shows that  $\mu_{pe}$  is zero when  $E < 0.5$ . Above  $E > 0.5$ , the electric force exerted on the condensed ions can overcome the friction force between the ions and the chain surface; hence there is relative motion between the ions and the chain.

In the fourth case, we study a salt concentration higher than the equivalence point. Figs. 13(a) and 13(b) present, respectively, the distributions of the condensed tetravalent counterions  $n_{+4}(i)$  and of the coions  $n_{-1}(i)$  on the chain at  $C_s = 6.0 \times 10^{-4}$ . The distribution of the monovalent counterion  $n_{+1}(i)$  is not shown because very few of them condense onto the chain.

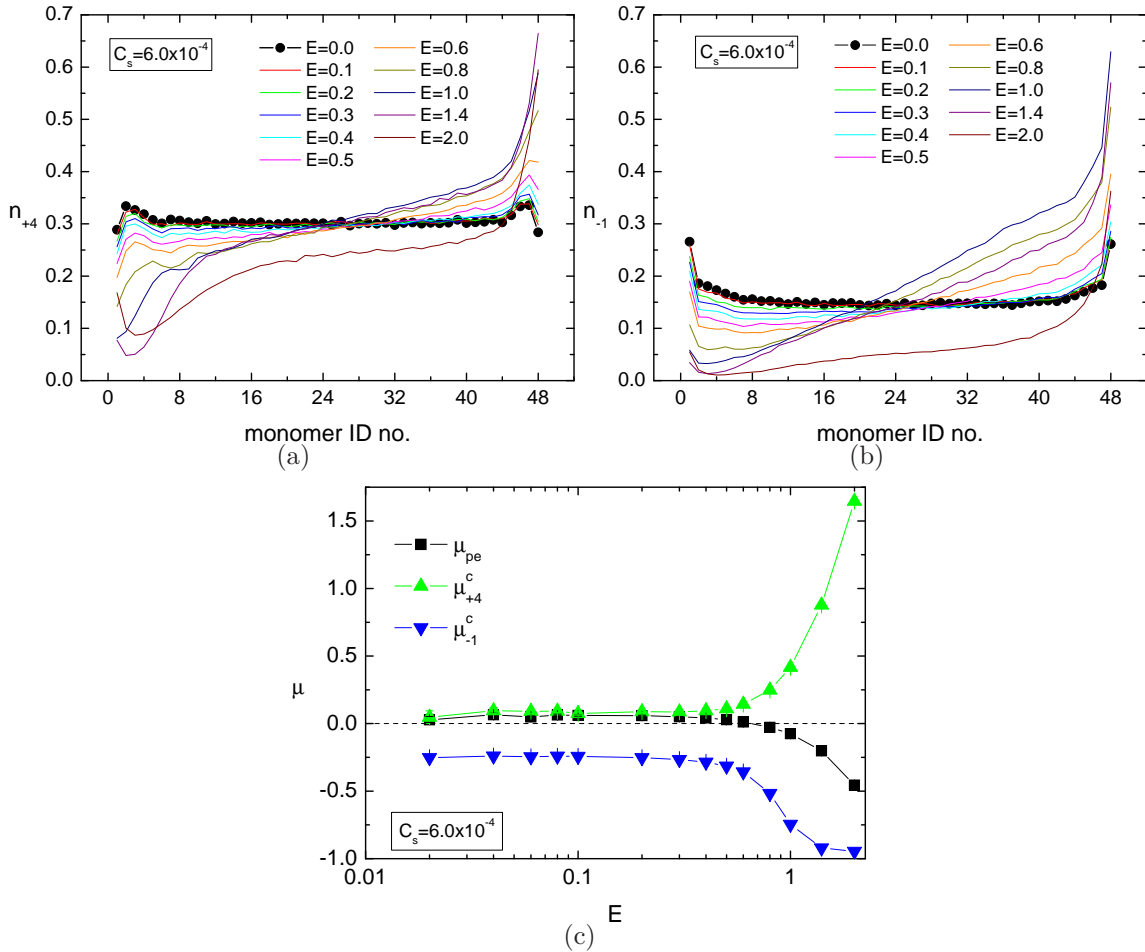


FIG. 13: (a) Distribution of condensed tetravalent counterions on chain,  $n_{+4}(i)$ , at  $C_s = 6.0 \times 10^{-4} (> C_s^*)$  in different electric fields  $E$ . The value of  $E$  can be read in the figure. (b) Same as (a), but for condensed coions  $n_{-1}(i)$ . (c) The mobility of the chain  $\mu_{pe}$ , of the condensed tetravalent counterions  $\mu_{+4}^c$ , and of the condensed coions  $\mu_{-1}^c$ , as a function of  $E$ .

The distribution  $n_{+4}(i)$  is similar to the one at  $C_s^*$  but the curve is shifted upward by a value of about 0.5. This upward-shifting shows that the number of the condensed tetravalent counterions exceeds the number needed to neutralize the chain. The chain is overcharged, and hence attracts coions onto it. The distribution  $n_{-1}(i)$  tilts when  $E$  is applied. The tilting is not toward the front end but rather toward the rear end and looks similar to  $n_{+4}(i)$ . It suggests that the condensation of the coions are, in fact, mediated by the condensed tetravalent counterions. The condensation of coion is weak because the mobility for the condensed coions  $\mu_{-1}^c$  is not zero even for the small set  $E$  fields simulated, as plotted in Fig. 13(c). The negative value of  $\mu_{-1}^c$  tells us that the condensed coions migrate constantly toward the chain front end. Surprisingly, the number of coions is less elevated at this end. This suggests that the chemical potential of the coion condensation is higher at this end. The tetravalent counterions condense more numerously at the rear of the chain, lowering the chemical potential there. The mobility  $\mu_{+4}^c$  is identical to  $\mu_{pe}^c$  when  $E < 0.5$ , which once again shows the strong condensation of tetravalent counterions. The tetravalent ions reside on the chain and move along with it. The positive value of the mobilities demonstrates that the effective chain charge becomes positive due to the over-condensation of tetravalent counterions. When  $E$  is strong enough to overcome the friction on the chain surface, the kinetics for the condensed ions and the chain are decoupled.  $\mu_{+4}^c$  increases but  $\mu_{pe}^c$  decreases. The magnitudes of the mobilities both increase.  $\mu_{-1}^c$  asymptotically approaches -1, the value expected for a coion drifting in the bulk solution.

We remark that the distributions of condensed ions studied here might be understood in the framework of sedimentation. In a dilute solution, sedimentation theory describes a barometric density profile  $\rho(z) = \rho_0 \exp(-z/L)$  for neutral particles, where  $z$  is the position in the gravitational direction and  $L = k_B T / (mg)$  is the characteristic length (also equal to the mean height of sediments) with  $m$  being the particle buoyant mass and  $g$  the gravitational acceleration. For charged particles, the mean height is shown to extend to  $ZL$  owing to electrostatic interactions [50, 51]. In our work, the condensed ions are under the action of an electric field, which can be analogously regarded as sedimenting in a gravitational field with the force  $mg$  effectively replaced by the net force  $ZeE - \xi F_n$  acting on a condensed ion. This analogy makes sense only when  $E$  is strong enough to displace the condensed ions and totally unfold the chain, so that the index  $i$  is linearly mapped to  $z$ . Following the index number in a reverse order, we observe that  $n_{+1}(i)$  in Fig. 10 displays as an exponential

function for  $E > 0.5$ , except near the two chain ends where some edge effect appears. The characteristic length  $L$  of the exponential can be seen to decrease with increasing  $E$ , which follows the depiction of the sedimentation theory. Similar results are found for  $n_{+4}(i)$  in Figs. 12 and 13 when  $E$  is strong. In the second case studied (in Fig. 11), we have two species of counterions condensing on the chain. Zwanikken and van Roij have developed a mean-field theory for the sedimentation of multicomponent charged colloids, based upon a Poisson-Boltzmann approach [52]. A segregation of layering charged colloids of valency  $Z_i$  was demonstrated, in which the order of the sediments, from the bottom to top, follow the increasing order of the product  $Z_i L_i$  [51, 52]. Since  $L_i = k_B T / (Z_i e E - \xi F_n)$  and  $F_n$  is approximately proportional to  $Z_i^2$ , the tetravalent counterions have a larger  $Z_i L_i$  than the monovalent ones. The theory thus predicts a profile along the chain which has the inverse order of what we obtained in the simulations. This difference arises because some mechanism cannot occur in mapping to a sedimentation system, for example, the dynamic condensation of counterions on a chain. The condensed monovalent counterions are stripped off in an electric field, more easily than the tetravalent ones. Consequently, the tetravalent counterions stay near the rear end of chain with longer time and the monovalent ones coming from the front are then stuck behind the tetravalent, which produces the observed profile.

### F. Dependence of chain mobility on chain length

Finally we studied the variation of chain mobility  $\mu_{pe}$  with chain length  $N$ , as the applied electric  $E$  increases. The results are presented in Fig. 14, panel (a) and (b), at two salt concentrations,  $C_s = 0.0$  and  $C_s^*$ , respectively, for  $N$  varying from 12 to 768. We have seen in Sec. III-C that the magnitude of  $\mu_{pe}$  largely increases when a chain unfolds.

Observe that the longer the chain length, the weaker the field strength that is needed to unfold the chain. Accompanying the unfolding,  $|\mu_{pe}|$  increases and the mobility reaches a constant value in the field region between  $E = 0.1$  and 1. For a stronger  $E$ , the magnitude of  $\mu_{pe}$  increases again. It is because the condensed ions can be further stripped off the chain, which renders the effective chain charge more negative, and thus, the chain drifts faster. The electric field required to change the chain mobility depends on the chain length. It provides a unique mechanism to electrophoretically separate PEs by  $N$ . Especially at  $C_s = C_s^*$ , the chains are initially neutralized by the multivalent counterions. They do not drift in

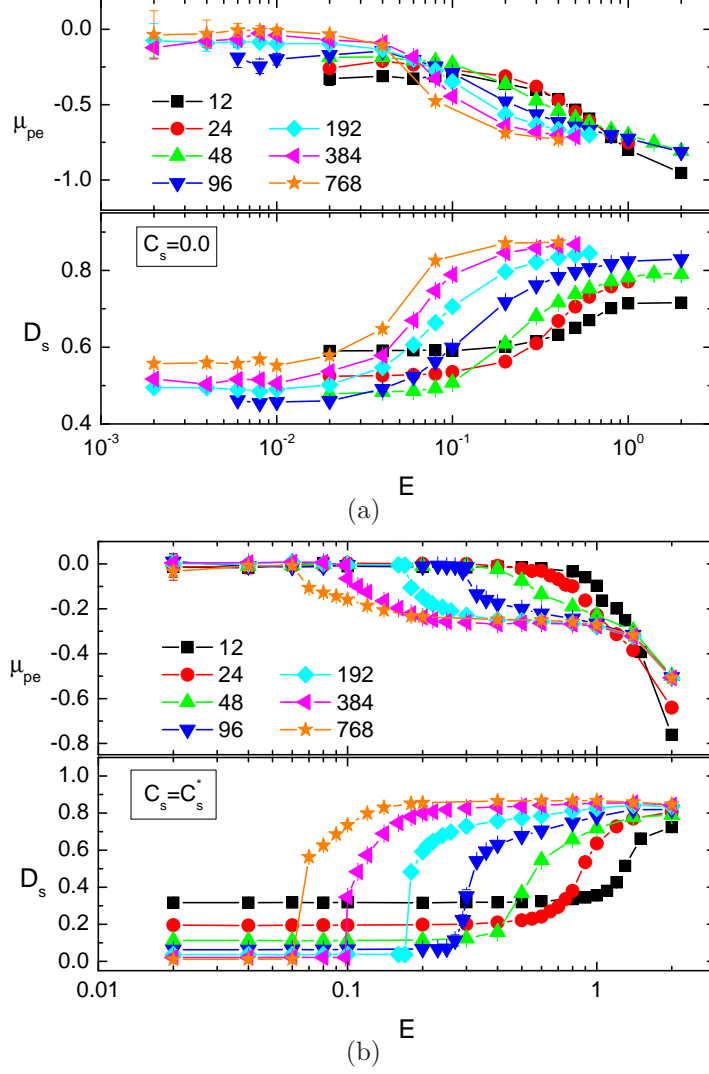


FIG. 14: Chain mobility  $\mu_{pe}$  and degree of chain unfolding  $D_s$  versus  $E$  (a) in salt-free solutions and (b) in solutions at equivalence point  $C_s^*$ . Each curve denotes the results run at one chain length  $N$  and the value of  $N$  is indicated in the upper panel.

weak fields. When an appropriate electric field is applied, the longer chains unfold and gain mobility, and as a consequence, drift away and are separated from the shorter chains.

Netz predicted that the unfolding electric field  $E^*$  should scale as  $N^{-3\nu/2}$  where  $\nu$  is the swelling exponent of chain size. We found in Fig. 14 that the chain unfolding, and also the mobility change, are not sharp transitions in electric fields. Consequently, it is not easy to determine the onset electric field for chain unfolding,  $E_{II}^*$ , with a good accuracy. Therefore, to verify the Netz' prediction, we calculated, in addition, the electric field  $E_{III}^*$ , which is the inflection point on the  $D_s$ -curve. The results are plotted in Fig. 15 as a function of  $N$ ,

together with  $E_I^*$  and  $E_{II}^*$ .

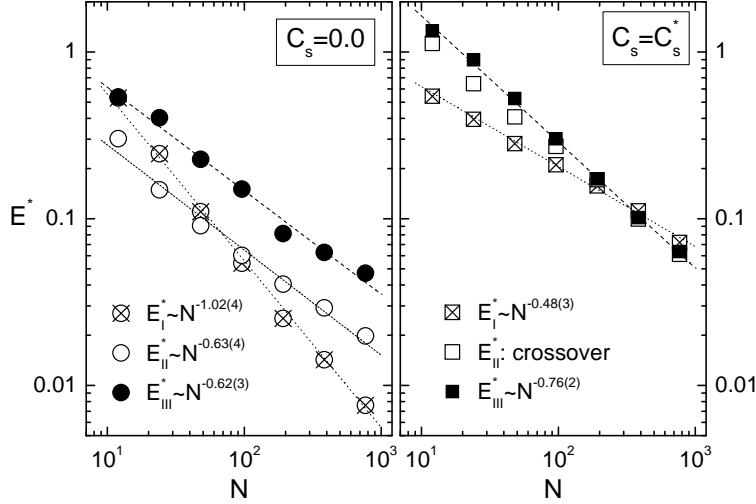


FIG. 15: Critical electric field  $E^*$  as a function of chain length  $N$  for  $C_s = 0.0$  and  $C_s = C_s^*$ .  $E^*$  is determined by the three ways: (1) the polarization energy equal to  $k_B T$ , (2) the onset point of  $D_s$ , and (3) the inflection point of  $D_s$ . The three estimators are denoted by  $E_I^*$ ,  $E_{II}^*$ , and  $E_{III}^*$ , respectively.

The three data sets at  $C_s = 0.0$  lie on straight lines in the log-log plot: The critical electric field does indeed follow a power-law function. Linear least-square fit yields that  $E_I^*$  scales as  $N^{-1.02(4)}$ ,  $E_{II}^*$  as  $N^{-0.63(4)}$ , and  $E_{III}^*$  as  $N^{-0.62(3)}$ . The scaling law for  $E_I^*$  is a refinement of our previous work [19]. It behaves differently to  $E_{II}^*$ , which is calculated directly from the chain size variation, and thus fails to predict the threshold field to unfold a chain. The failure arises from oversimplified setting of the critical polarization energy for chain unfolding  $W_{pol}^*$  to the thermal energy  $k_B T$ , which should be also a function of chain length and salt concentration, as shown in Fig. 6. The two fitting lines for  $E_{II}^*$  and  $E_{III}^*$  run parallel to each other. Consequently, the ratio of  $E_{III}^*$  to  $E_{II}^*$  is a constant, suggesting that either measure of  $E^*$  is acceptable. At  $C_s = C_s^*$ ,  $E_I^*$  scales as  $N^{-0.48(3)}$ , a wrong prediction for the unfolding field. For  $E_{II}^*$  and  $E_{III}^*$ , markedly different behavior is observed. Only the  $E_{III}^*$  data follow a scaling law with the exponent equal to  $-0.76(2)$ . The onset field point  $E_{II}^*$  exhibits a crossover from an exponent close to  $-0.63$  at small polymerizations to  $-0.76$  when  $N > 100$  which agrees with the  $E_{III}^*$  value. This crossover reflects the fact that the transition of chain unfolding becomes sharper when chain length increases, as seen in Fig. 14(b).

To check Netz' theory [7, 8], we calculate the swelling exponent  $\nu$  of chains in the zero field limit through the scaling relation  $R_g^2 \sim N^{2\nu}$ . Our simulations show that  $\nu = 0.92(1)$  at  $C_s = 0.0$  and  $\nu = 0.33(1)$  at  $C_s = C_s^*$ . Therefore, according to Netz, the critical field should scale as  $N^{-1.38(2)}$  and  $N^{-0.50(2)}$ , respectively. However, the scaling law obtained in Fig. 15 differs from the prediction. The modified Netz' theory that considers PEs as ellipsoidal objects predicts that the critical electric field scales as  $V^{-1/2}$  where  $V$  is calculated from the eigenvalues of the gyration tensor [19]. Our refining results show that  $V \sim N^{2.44(1)}$  for  $C_s = 0.0$  and  $V \sim N^{1.13(1)}$  for  $C_s = C_s^*$  in zero fields. The modified Netz' theory hence predicts  $E^* \sim N^{-1.22(1)}$  and  $E^* \sim N^{-0.56(1)}$ , which are, again, inconsistent with the results of Fig.15. The differences are so important that a new and detailed understanding of the mechanism of chain unfolding is necessary. It is definitely a topic worthy to be investigated in the future.

We remark that Netz' original work does not verify the scaling of  $E^*$  with chain length. Moreover, the PE was collapsed by monovalent counterions ( $q = 1$ ) due to the assumption of a large Coulomb coupling constant  $\Xi = \lambda_B q^2 / \sigma$ , ranging between 5 and 30. The situation is equivalent to a collapsed PE in a (1:1)-salt solution at very low temperature because the Bjerrum length  $\lambda_B$  is large, with a value lying between  $5\sigma$  to  $30\sigma$ . In the derivation, no multivalent counterions were considered, neither was the competition between multivalent ions and monovalent ones as happens in reality. Therefore, the disagreement with our results arises from these simplified assumptions in the model. In the theory, the critical polarization energy is equal to  $k_B T$ , which has to be improved. Moreover, the transition is assumed to be sharp. Our simulations reveal a more complicated story: The chain conformational transition is a continuous change at  $C_s = 0.0$ , while it is a more discontinuous transition at  $C_s = C_s^*$ , particularly when  $N$  is large. Therefore, the onset critical field  $E_{II}^*$  and the inflection critical field  $E_{III}^*$  follow different scaling laws in different solutions. The ratio between the two estimators describes the sharpness of the transition and theory should account for its deviation from unity.

In our previous work [20], the critical electric field in trivalent salt solutions at the equivalence point was studied through the inflection-point method. The scaling exponent was found to be  $-0.77(1)$ , which is consistent with what we obtain here. This seems to suggest that the inflection critical field for trivalent and for tetravalent salts follows a similar scaling law. Liu et al. have recently studied the scaling law of DC unfolding fields in monovalent,

divalent, and trivalent salt solutions by simulations [21]. The exponents reported depended on the salt valency. The result for trivalent salt ( $-0.64$ ) at equivalence point is not consistent with ours. Since the chain length is short in their study (only up to  $N = 192$  in comparison with ours  $N = 768$ ) and the inflection point is ambiguous (see Fig. 3 in the paper), their results are not reliable. However, the study gives rise a relevant and interesting question: Does the critical electric field follow a different scaling law when the valency of salt is small, such as monovalent and divalent salt, as claimed? It necessitates a detailed and precise investigation in the future. According to our work, the unfolding electric field shares a similar scaling exponent in trivalent and tetravalent salt systems but the prefactor in the scaling law is different. Many phenomena in both of the systems occur in a similar way, such as ion distributions and mobility changes.

We study the tetravalent system because large ion valency can give a stronger response to applied electric fields, which makes observing the effects easier. From the point of view of applications, it is very important to understand the role of salt valency in PE solutions in electric fields. The selection of salt valency depends on the research context and goal. We hope that the information reported here can be helpful in the development of techniques for molecular separation and in the design of functionalized micro/nano-fluidic devices.

#### IV. CONCLUSIONS

In this work, we performed molecular dynamics simulations to investigate the conformational and electrophoretic properties of chains in tetravalent salt solutions subject to electric fields. Our results show that chain size depends strongly on the salt concentration  $C_s$  and that under the action of electric fields, the chain shape can be altered. When the field strength is stronger than a critical value  $E^*$ , the chains are largely extended to an elongated structure. Two estimators  $E_I^*$  and  $E_{II}^*$  were used to calculate  $E^*$  through equating  $W_{pol}$  to  $k_B T$  and identifying the onset point of  $D_s$ , respectively. The obtained values show that  $E^*$  is a non-monotonic function of  $C_s$ , and the maximum value appears at the equivalence point  $C_s = C_s^*$ . The dipole moment shows that chain polarization displays a linear dependence on the electric field up to  $E_{II}^*$ .

The salt concentration has a strong influence on the electrophoretic mobility of the chain and ion distributions. In weak electric fields, the chain mobility  $\mu_{pe}$  is negative for  $C_s < C_s^*$ ,



whereas it is positive when  $C_s > C_s^*$ . The latter demonstrates the sign inversion of the effective chain charge. The mobility of the condensed tetravalent counterions  $\mu_{+4}^c$  is identical to  $\mu_{pe}$  because the condensed ions are tightly bound onto the chains and move together in the electric fields. When the applied electric field  $E$  is stronger than  $E_{II}^*$ , the chains unfold such that  $\mu_{+4}^c$  and  $\mu_{pe}$  are no longer identical. In an even higher  $E$  field,  $\mu_{+4}^c$  becomes positive and  $\mu_{pe}$  becomes negative: There is a relative motion between the chains and the condensed tetravalent ions. The number of the condensed ions shows that part of the condensed tetravalent ions are stripped-off from the chains due to the strong electric fields. The behavior of the effective chain charge  $Q$  is consistent with the chain mobility found.

Moreover, we studied in detail the distribution of different species of ions condensed on the chains. The counterions are dragged toward the rear of the chain, due to the polarization. For  $C_s < C_s^*$ , the condensation profile displays that the tetravalent counterions condense at the chain rear, followed by the condensed monovalent ones right behind the tetravalent, close to the chain center, owing to the strong electrostatic repulsion between the counterions. For  $C_s \geq C_s^*$ , monovalent counterions are totally expelled from the chain, which leaves only the condensed tetravalent counterions, which overcharge the surface of the chains due to the excessive condensation. Consequently, the coions are attracted to the chains and condensed. This process is mediated by the condensed tetravalent counterions because a similar profile of coion distribution to the tetravalent one is found. An analogy of our system to sedimentation problems was used to explain the ion condensation profile.

Finally, we investigated the dependence of chain mobility and unfolding transition on the chain length  $N$ . The estimator  $E_{III}^*$  was considered through the calculation of the inflection point of  $D_s$ . At  $C_s = 0.0$ , the transition of chain size is not sharp. But  $E_{II}^*$  and  $E_{III}^*$  follow a similar scaling law  $N^{-0.63(4)}$  with different prefactors. However, at the equivalence point, the unfolding transition becomes sharper.  $E_{III}^*$  scales as  $N^{-0.76(2)}$ . A crossover was observed in  $E_{II}^*$ , which converges asymptotically to  $E_{III}^*$  when  $N$  is large. The scaling laws obtained here are significantly different to both Netz' prediction and the modified theory. Noticeably,  $E_I^*$  fails to predict the unfolding field, which shows that the critical polarization energy is not simply  $k_B T$ . It hence necessitates a further investigations to explore the mechanism of chain unfolding in electric fields and the associated mobility and electrokinetics changes.

## Acknowledgments

We thank T. N. Shendruk for reading the manuscript and discussing. This material is based upon work supported by the National Science Council, the Republic of China, under Grant No. NSC 97-2112-M-007-007-MY3. Computing resources are supported by the National Center for High-performance Computing.

- 
- [1] H.-C. Chang and L. Y. Yeo, *Electrokinetically Driven Microfluidics and Nanofluidics* (Cambridge, 2010).
  - [2] H. Cottet and J.-L. Viovy, *Electrophoresis* **19**, 2151 (1998).
  - [3] J.-L. Viovy, *Rev. Mod. Phys.* **72**, 813 (2000).
  - [4] P. Mayer, G.-W. Slater, and G. Drouin, *Anal. Chem.* **66**, 1777 (1994).
  - [5] T. N. Shendruk, O. A. Hickey, G. W. Slater, and J. L. Harden, “Electrophoresis: When Hydrodynamics Matter”, to appear in *Curr. Opin. Colloid Interface Sci.*
  - [6] G. W. Slater, *Electrophoresis* **30**, S181 (2009).
  - [7] R. R. Netz, *Phys. Rev. Lett.* **90**, 128104 (2003).
  - [8] R. R. Netz, *J. Phys. Chem. B* **107**, 8208 (2003).
  - [9] V. A. Bloomfield, *Curr. Opin. Struct. Biol.* **6**, 334 (1996).
  - [10] V. A. Bloomfield, *Biopolymers* **44**, 269 (1997).
  - [11] A. Y. Grosberg, T. T. Nguyen, and V. I. Shklovskii, *Rev. Mod. Phys.* **74**, 329 (2002).
  - [12] M. Quesada-Perez, E. Gonzalez-Tovar, A. Martin-Molina, M. Lozada-Cassou, and R. Hidalgo-Alvarez, *ChemPhysChem* **4**, 235 (2003).
  - [13] C. C. Conwell, I. D. Vilfan, and N. V. Hud, *Proc. Natl. Acad. Sci. USA* **100**, 9296 (2003).
  - [14] Y.-F. Wei and P.-Y. Hsiao, *J. Chem. Phys.* **132**, 024905 (2010).
  - [15] T. T. Nguyen, I. Rouzina, and B. I. Shklovskii, *J. Chem. Phys.* **112**, 2562 (2000).
  - [16] P.-Y. Hsiao, *J. Phys. Chem. B* **112**, 7347 (2008).
  - [17] V. Vijayanathan, T. Thomas, and T. J. Thomas, *Biochem.* **41**, 14085 (2002).
  - [18] D. Porschke, *Biopolymers* **24**, 1981 (1985).
  - [19] P.-Y. Hsiao and K.-M. Wu, *J. Phys. Chem. B* **112**, 13177 (2008).
  - [20] Y.-F. Wei and P.-Y. Hsiao, *Biomicrofluidics* **3**, 022410 (2009).

- [21] H. Liu, Y. Zhu, and E. Maginn, *Macromolecules* **43**, 4805 (2010).
- [22] E. Y. Chan, *Mutat. Res. -Fundam. Mol. Mech. Mutagen.* **573**, 13 (2005).
- [23] P. K. Gupta, *Trends Biotechnol.* **26**, 602 (2008).
- [24] R. Treffer, *Curr. Opin. Biotechnol.* **21**, 4 (2010).
- [25] P.-Y. Hsiao, Y.-F. Wei, and H.-C. Chang, *Soft Matter* **7**, 1207 (2011).
- [26] S. Wang, H.-C. Chang, and Y. Zhu, *Macromolecules* **43**, 7402 (2010).
- [27] Y.-F. Wei and P.-Y. Hsiao, *J. Chem. Phys.* **127**, 064901 (2007).
- [28] P.-Y. Hsiao, *J. Chem. Phys.* **124**, 044904 (2006).
- [29] P.-Y. Hsiao, *Macromolecules* **39**, 7125 (2006).
- [30] P.-Y. Hsiao and E. Luijten, *Phys. Rev. Lett.* **97**, 148301 (2006).
- [31] L. C. McCormick and G.-W. Slater, *Electrophoresis* **28**, 674 (2007).
- [32] L. C. McCormick and G.-W. Slater, *Electrophoresis* **28**, 3837 (2007).
- [33] R. W. Hockney and J. Y. Eastwood, *Computer Simulation Using Particles* (Taylor & Francis, 1988).
- [34] M. Rubinstein and R. Colby, *Polymer Physics* (Oxford, 2003).
- [35] The simulations were run using modified LAMMPS package (<http://lammmps.sandia.gov/>).
- [36] D. Long, J.-L. Viovy, and A. Ajdari, *Phys. Rev. Lett.* **76**, 3858 (1996).
- [37] M. Tanaka and A. Y. Grosberg, *Eur. Phys. J. E* **7**, 371 (2002).
- [38] M. Tanaka, *Phys. Rev. E* **68**, 061501 (2003).
- [39] K. Grass and C. Holm, *Soft Matter* **5**, 2079 (2009).
- [40] F. J. Solis and M. O. de la Cruz, *J. Chem. Phys.* **112**, 2030 (2000).
- [41] F. J. Solis and M. O. de la Cruz, *Eur. Phys. J. E* **4**, 143 (2001).
- [42] F. J. Solis, *J. Chem. Phys.* **117**, 9009 (2002).
- [43] M. O. de la Cruz, L. Belloni, M. Delsanti, J. P. Dalbiez, O. Spalla, and M. Drifford, *J. Chem. Phys.* **103**, 5781 (1995).
- [44] E. Raspaud, M. O. de la Cruz, J.-L. Sikorav, and F. Livolant, *Biophys. J.* **74**, 381 (1998).
- [45] M. Bishop and C. J. Saltiel, *J. Chem. Phys.* **88**, 6594 (1988).
- [46] G. S. Manning, *J. Chem. Phys.* **51**, 924 (1969).
- [47] H. R. Kruyt, *Ed. Colloid Science*, vol. Vol. II (Elsevier Publishing Company: New York, 1949).
- [48] M. Elimelech and C. R. O'Melia, *Colloids Surf.* **44**, 165 (1990).

- [49] M. de Frutos, E. Raspaud, A. Leforestier, and F. Livolant, *Biophys. J.* **81**, 1127 (2001).
- [50] R. van Roij, *J. Phys.:Condens. Matter* **15**, S3569 (2003).
- [51] A. Cuetos, A.-P. Hynninen, J. Zwanikken, R. van Roij, and M. Dijkstra, *Phys. Rev. E* **73**, 061402 (2006).
- [52] J. Zwanikken and R. van Roij, *Europhys. Lett.* **71**, 480 (2005).